Early-life stress induces persistent astrocyte dysfunction resulting in fear generalisation.

Authors: Mathias Guayasamin[1,2,*], Lewis R. Depaauw-Holt[1,2,*], Ifeoluwa I. Adedipe[1,2,*], Ossama Ghenissa[1,2], Juliette Vaugeois[1,2], Manon Duquenne[1,2], Benjamin Rogers[1,2], Jade Latraverse-Arquilla[2], Sarah Peyrard[2], Anthony Bosson[2] and Ciaran Murphy-Royal[1,2,‡].

Affiliations:

1. Département de Neurosciences, Université de Montréal, Montréal, Québec, Canada.
2. Centre de Recherche du Centre Hospitalier de l'Université de Montréal (CRCHUM), Montréal, Québec, Canada

* Co-first authors

‡ Corresponding author

Corresponding author: Ciaran Murphy-Royal (ciaran.murphy-royal@umontreal.ca)
CRCHUM, 900 rue st Denis, Montéal, Québec, Canada, H2X 0A9

Abstract

Early-life stress can have lifelong consequences, enhancing stress susceptibility and resulting in behavioral and cognitive deficits. While the effects of early-life stress on neuronal function have been well-described, we still know very little about the contribution of non-neuronal brain cells. Investigating the complex interactions between distinct brain cell types is critical to fully understand how cellular changes manifest as behavioral deficits following early-life stress.
Here, using male and female mice we report that early-life stress induces anxiety-like behavior and fear generalisation in an amygdala-dependent learning and memory task. These behavioral changes were associated with impaired synaptic plasticity, increased neural excitability, and astrocyte dysfunction. Genetic perturbation of amygdala astrocyte function by either silencing these cells or reducing astrocyte network function was sufficient to replicate cellular, synaptic, and fear memory changes associated with early-life stress.
These data provide mechanistic links between early-life stress and astrocyte dysfunction. Our data reveal a role of astrocytes in tuning emotionally salient memory with astrocyte dysfunction resulting in fear generalisation. Further understanding of how astrocytes are affected by stress might offer new insights into the long-term impact of early-life stress on affective states.

Keywords

Astrocytes, early-life stress, learning and memory, fear discrimination, amygdala, synaptic plasticity, neuronal excitability.

Short title

Long-term astrocyte dysfunction in early-life stress

Introduction

Both human and rodent studies have provided compelling evidence for the long-lasting effects of adverse early-life experiences, highlighting enhanced susceptibility to subsequent stressors later in life (1–5). Early-life stress (ELS) has widespread effects across the brain and can influence many neural circuits including those involved in threat detection, emotion, cognitive processing, and reward seeking behaviors (6–9). Research investigating the neurobiology of stress has predominantly focused upon investigating the effects on neurons and the consequences for behavior (10–19). We have gleaned tremendous insight into disorders of stress from these studies, yet the links between stress, brain circuits and behavior remain tenuous. Within this framework, the contribution of distinct brain cells, including astrocytes, remains largely untested. Glial cells, which comprise approximately half the cell population in the brain have been shown to directly regulate synaptic transmission and plasticity (20–27), thereby influencing many discrete behaviors (23,28,30–32,34,36). Despite research suggesting important roles for astrocytes in regulating affective states (29), fear (31), and reward seeking behaviors (33,35), whether astrocyte dysfunction prompts stress-induced behavioral impairments remains poorly understood.

First, we characterised whether ELS influenced stress hormone levels across our experimental paradigm from pre-stress until young adulthood. We report that ELS induces a transient increase in blood glucocorticoids that peaks during late adolescence/young adulthood. Turning to behaviour, this increase in glucocorticoid levels was associated with anxiety-like behavior in open field test and elevated plus maze.

Next, we next set out to determine whether ELS induces cognitive impairment using an amygdala-dependent threat discrimination assay. This task was specifically chosen to test the effects of ELS on amygdala function as this brain region is involved with threat detection and associative learning that is acutely sensitive to stress (17,18,37–39). We employed an auditory discriminative fear conditioning paradigm that requires synaptic plasticity changes in the lateral amygdala (40) and found that ELS impairs discriminative fear memory, specifically we found fear generalisation in ELS mice. These hormonal and behavioral changes were associated with impaired synaptic plasticity and enhanced excitability of cells in the lateral amygdala, evidenced by increased c-Fos labelling.

Finally, we investigated the impact of ELS on astrocytes in the lateral amygdala revealing changes in specific proteins associated morphological reorganisation and astrocyte network function. To directly implicate astrocytes with behavioral dysfunction we used two distinct viral approaches to genetically disrupt astrocyte function specifically in the lateral amygdala. These astrocyte-specific manipulations recapitulated ELS-induced fear generalisation, synaptic, and excitability phenotypes supporting the hypothesis that astrocytes play an influential role in the effects of stress on neural circuits and behavior. Together, these findings identify astrocytes as central elements regulating amygdala-dependent affective memory and highlight astrocytes as putative targets for the treatment of stress disorders.

Results

ELS increases blood corticosterone and induces anxiety-like behaviors.

45 We employed an ELS paradigm which combines limited bedding and nesting materials as well as maternal separation from postnatal days 10 to 17 (**Figure 1A**). This ELS paradigm has been shown to induce life-long stress susceptibility (6). We first set out to determine the impact of this ELS paradigm on stress hormone levels across our experimental window. We took trunk blood from mice across several litters at different time points in the ELS paradigm: pre-stress
50 (P10), end of ELS paradigm (P17), at the start (P45) and end of our experimental window (P70). We report that this ELS paradigm induces a latent increase in blood corticosterone with a significant increase occurring only in late adolescence P45, long after the termination of the stress paradigm (**Figure 1B**).

Next, we measured whether this ELS paradigm, associated with high corticosterone results
55 in long-term changes in anxiety-like behaviors. We found that while there were no changes in behavior in the open-field task (**Figure 1C, D**), we did see an increase in locomotor activity, i.e. distance travelled, following ELS (**Figure 1E**). Using the elevated plus maze we report increased anxiety-like behavior with a reduction in open-closed arm ration, where a value of 1.0 would indicate equal time spent in each compartment (**Figure 1F, G**). This was
60 accompanied by an increase in distance travelled within the maze (**Figure 1H**), similar to our findings in the open field. Increased locomotion in response to stress is consistent with previous reports (15).

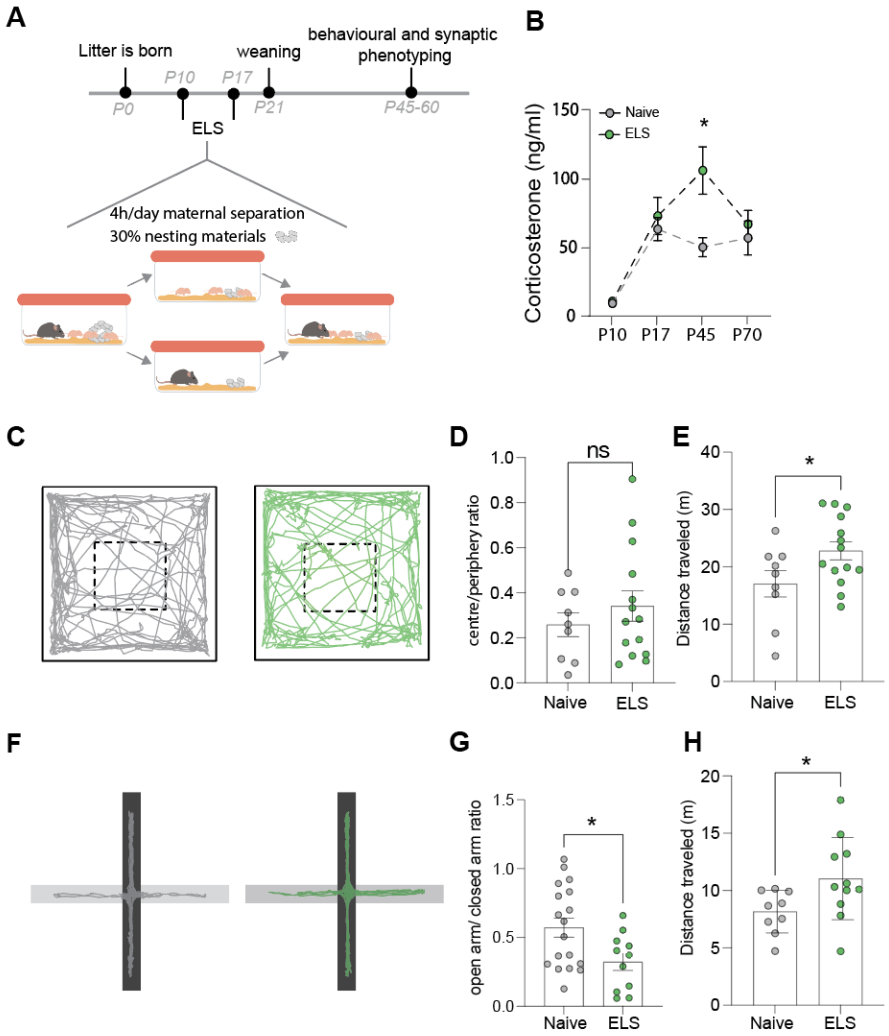

Figure 1. Effects of ELS on anxiety-like behaviour.

(A) Timeline of ELS and behavioural assays. **(B)** Serum corticosterone levels are increased during adolescence, following ELS. P=0.01, Naïve N=9, ELS N=11 mice. **(C)** Representative movement tracks of naive (grey) and ELS (green) mice in open field task. **(D)** No significant difference in centre/periphery ratio in open field following ELS. P=0.39, Naïve N=9, ELS N=14 mice. **(E)** Total distance travelled during open field test was increased in ELS mice. P=0.04, Naïve N=9, ELS N=14 mice. **(F)** Representative locomotor tracks in elevated plus maze in naïve and ELS mice, black segment represents closed arms with grey arms representing open arms. **(G)** ELS mice had a reduced open/closed arm ratio. P=0.02, Naïve N=18, ELS N=11 mice. **(H)** Total distance travelled during elevated plus maze test was increased by ELS. P=0.02, Naïve N=9, ELS N=11 mice. See Table S1 for detailed statistical summaries.

Amygdala-dependent memory, plasticity, and excitability are affected by ELS.

Considering the strong association between stress disorders, anxiety, and amygdala dysfunction, we next set out to determine whether amygdala-dependent behavior was impacted by ELS. We specifically targeted lateral amygdala-dependent learning and memory using an auditory discriminative fear conditioning paradigm. In brief, during this behavioral task mice are first exposed to a neutral auditory cue (conditioned stimulus - ; CS-) and then an

aversive cue (CS+) paired with footshock (unconditioned stimulus; US;). On day two mice are placed in a novel environment to remove contextual triggers and exposed to auditory cues from previous day without footshock (**Figure 2A**). Learning and memory were measured using percent time freezing during presentation of auditory cues. We report that mice accurately learn this task and can readily distinguish between neutral and aversive cues (see **Table S1**).

Using this paradigm our data show no difference in freezing responses to the CS- presentations during conditioning between naïve and ELS mice (**Figure 2B, grey area**). This suggest that ELS does not induce hypersensitivity or hypervigilance to novel auditory cues. We also show that fear acquisition, evidenced by freezing to the CS+/US pairing, is also unaffected by ELS (**Figure 2B**). In contrast, memory recall was affected by stress with ELS mice showing enhanced freezing responses to neutral cues (CS-, **Figure 2C, grey area**), with no difference in fear responses to aversive cues (CS+; **Figure 2C**) between ELS and naïve mice. Enhanced freezing to neutral auditory cues by ELS mice is indicative of fear generalisation, a common stress-related behavioural phenotype conserved between rodents and humans(41,42). This behavioural observation is more clearly depicted using a discrimination index (DI) that takes into account freezing responses to neutral and aversive cues. Using this measure, DI>0 reflects accurate discrimination, DI=0 no discrimination and DI<0 reflects a discrimination error i.e. higher freezing to the neutral than aversive tone. Using this index, we reveal a significant decrease in fear discrimination in ELS mice compared to naïve mice (**Figure 2D**). This ELS-induced decrease in discrimination can be accounted for by increased freezing to the neutral cue since there are no significant differences in freezing to the aversive cue between ELS and naïve animals. Together these data suggest that ELS enhances affective responses to neutral/non-aversive cues, resulting in fear generalisation in adult mice. Importantly, we

observed no differences between male and female mice in this paradigm with both sexes showing equal performance in learning (**Figure S1A**), memory (**Figures S1B**), and auditory discrimination (**Figure S1C**) and use both sexes in all experiments.

Amygdala-dependent auditory fear conditioning has been consistently correlated with the potentiation of lateral amygdala post-synaptic responses to auditory afferents originating from the cortex and the thalamus (35). Click or tap here to enter text.As such, we set out to determine whether ELS impacts synaptic plasticity in cortico-amygdala circuits using acute brain slice electrophysiology and recorded field excitatory postsynaptic potentials (fEPSPs) by stimulating cortical inputs from the external capsule (**Figure 2E**). We found that ELS results in decreased long-term potentiation (LTP) of synaptic transmission in this cortico-amygdala circuit (**Figures 2F,G** and **S1D**). This synaptic observation is consistent with findings using distinct stress paradigms (20), and highlights the important influence of stress on synaptic function across various brain regions.

Fear learning and memory in the LA have also been correlated with the allocation of small subsets of neurons to a fear engram (40). These engrams are thought to be a possible neural substrate for memory (36–37) and their formation depends on neural excitability levels at the moment of acquisition. To reveal stress-induced changes in neural excitability, we collected brain tissue 90 minutes after conditioning paradigm (**Figure 2H**), and carried out immunostaining for the immediate early gene c-Fos, a commonly used activity marker, in the lateral amygdala (**Figures 2I,J,** and **S1E,F**). Fear acquisition in the ELS group resulted in a significant increase in c-Fos density suggestive of increased excitability levels. These results are consistent with other reports of discriminative memory and c-Fos density, with c-Fos density inversely correlated with memory accuracy (45).

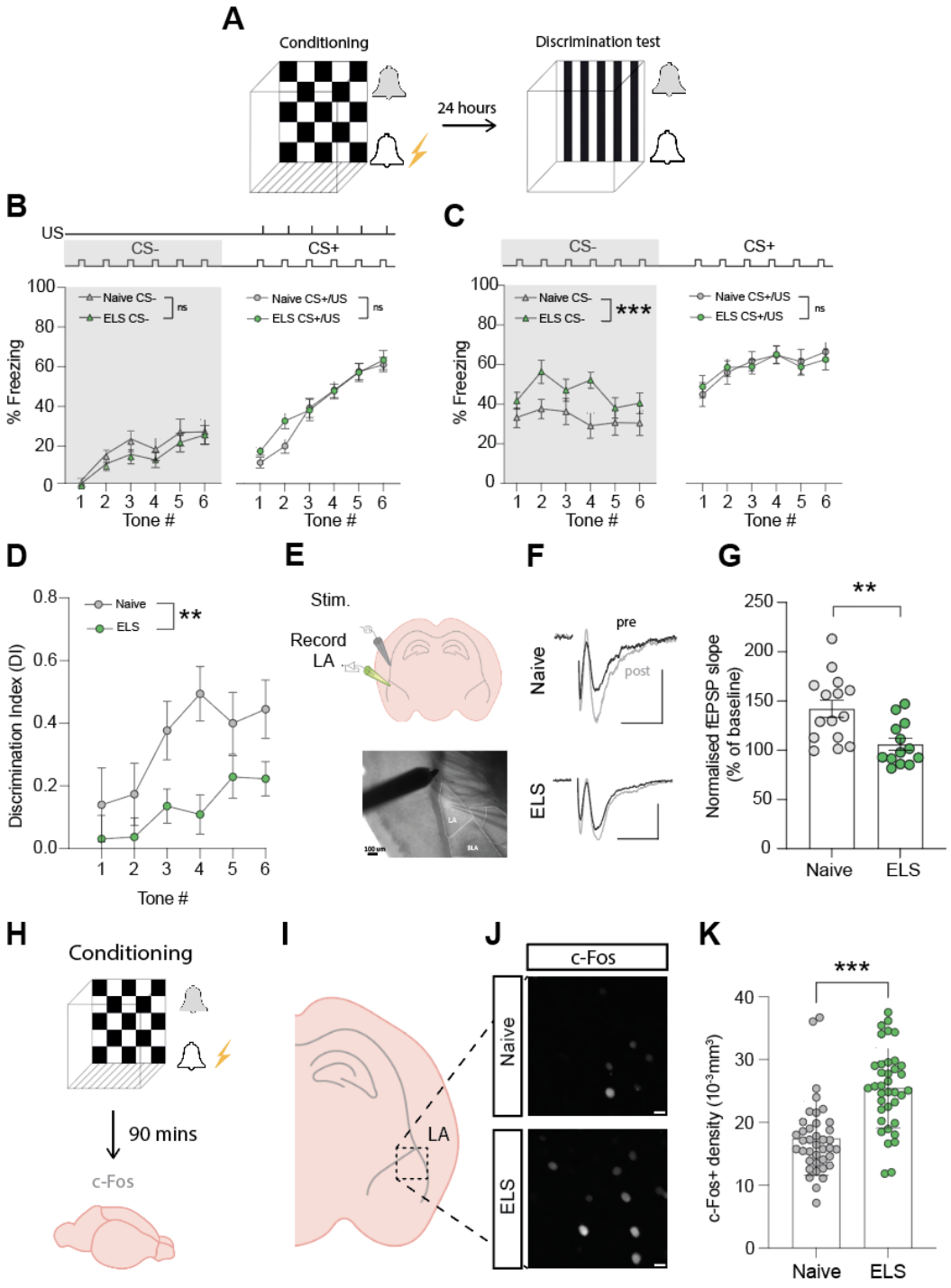

120 **Figure 2. ELS alters fear memory, synaptic plasticity, and excitability.**

(A) Timeline of auditory discriminative fear conditioning paradigm. **(B)** ELS did not affect % Freezing to neutral and aversive auditory cues during learning. Naïve N=20, ELS N=17. **(C)** % time freezing during presentation of neutral auditory cue (CS-; p=0.0002) and aversive cue (CS+; p=0.99). Naïve N=20, ELS

N=17. **(D)** Discrimination Index was impaired by ELS. P=0.004. Naïve N=20, ELS N=17. **(E)** Schematic representation of electrode placement in slice electrophysiology experiment (top) with DIC image below. **(F)** Representative EPSP traces from naïve (top) and ELS (bottom) brain slices during baseline (black trace) and after LTP stimulation (grey trace). Scale bars = 0.5mV and 10ms. **(G)** LTP was impaired by ELS. P=0.002. Naïve N=15, ELS N=13. **(H)** Diagram of procedure for c-fos staining experiments. **(I)** Brain slices containing lateral amygdala (LA) were selected for c-Fos staining. **(J)** Region of interested extracted from full amygdala image. Scale bars = 10μm. **(K)** c-Fos positive cell density was increased by ELS. P<0.0001. Naïve n=39 slices N=10 mice, ELS n=37 slices N=10mice. See Table S1 for detailed statistical summaries.

Early-life stress induces long-term astrocyte dysfunction.

To determine the influence of ELS on astrocytes in the lateral amygdala we carried out immunostaining on brain slices taken from young adult naïve and ELS mice. We first investigated whether increased blood corticosterone affects glucocorticoid receptor (GR) expression and localisation in astrocytes. Using immunostaining we found that this hormone receptor is abundantly expressed in lateral amygdala astrocytes (**Figure 3A**). We further investigated the subcellular localisation of GR within astrocytes. When inactivated GRs are restricted to the cytosol, upon binding to agonists such as corticosterone however, GRs can translocate to the nucleus to influence gene expression (46). Calculating a ratio of cytosolic vs nuclear GR in astrocytes as a proxy for activity, we found an increase in the nuclear fraction of GR in astrocytes following ELS (**Figure 3B**). These results are suggestive of increased activation of glucocorticoid signaling in lateral amygdala astrocytes following ELS.

To assess any potential changes in astrocyte structure and function we investigated expression of the intermediate filament protein glial fibrillary acidic protein (GFAP; **Figure 3C,D**) and found a significant decrease in GFAP fluorescence intensity in the LA following ELS (**Figure 3E**). While functional consequences of GFAP changes are difficult to define, we interpret these modifications in GFAP expression to be indicative of an astrocytic response to stress. To identify specific functional changes induced by ELS, we targeted astrocyte-specific proteins with known roles in influencing synaptic function including Cx43, a GAP-junction protein that composes astrocyte networks (47) and the glutamate transporter GLT-1, responsible for the efficient clearance of glutamate from the synaptic cleft (41; **Figure 3C,D**). We observed a decrease in fluorescence intensity for Cx43 (**Figure 3F**) while GLT-1 remained

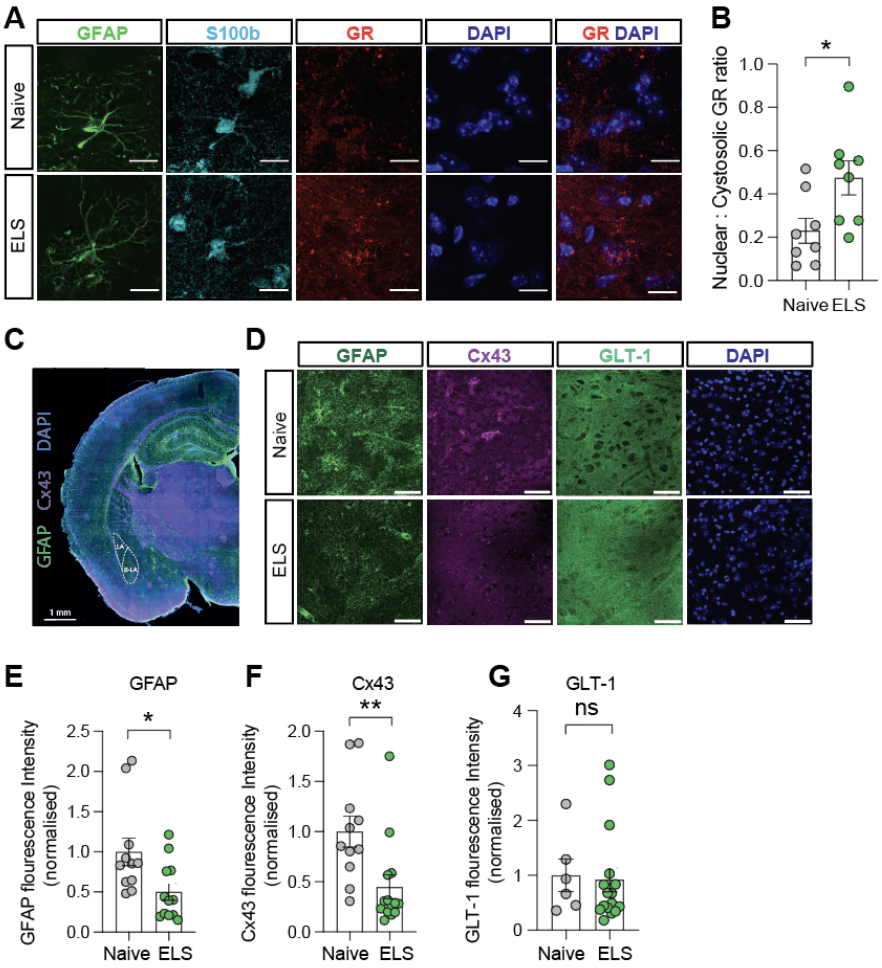

Figure 3. Long-term astrocyte dysfunction after early-life stress. **(A)** Representative immunostaining of GFAP, S100b, GR, DAPI, and GR/DAPI merge in Naïve and ELS conditions. Scale bars = 20µm **(B)** Nuclear/cystolic GR ratio in astrocytes was increased after ELS. P=0.026. Naïve N=8, ELS N=8. **(C)** Representative slide scan image of immunostaining for astrocyte proteins GFAP and Cx43. **(D)** Representative immunostaining of GFAP, Cx43, GLT-1, and DAPI in naïve and ELS conditions. Scale bars = 50µm **(E)** GFAP staining was reduced in ELS mice. p=0.02, Naïve N=11, ELS N=12. **(F)** Cx43 staining was decreased in ELS mice. p=0.008. Naïve N=11, ELS=14. **(G)** GLT-1 expression was unchanged by ELS. P=0.8. Naïve N=6, ELS N=16. See Table S1 for detailed statistical summaries.

unaffected by ELS (**Figure3G**). These data suggest that astrocytes mount a specific response to ELS which could result in discrete changes in astrocyte network function such as the uncoupling of the astrocytic Cx43 GAP-junction networks in the lateral amygdala.

Astrocyte dysfunction alone is sufficient to phenocopy the effects of ELS on fear generalisation, synaptic plasticity, and excitability.

To implicate astrocytes in the cellular and behavioral effects of ELS we carried out a series of genetic loss-of-function experiments, specifically targeting astrocytes in the lateral amygdala using viral approaches (**Figure 4A** and **S2A**). Based on the putative astrocyte network dysfunction we identified in fixed tissue (**Figure 3F**), we targeted astrocyte network function by overexpressing a dominant negative Cx43 (dnCx43). We have previously shown this manipulation to completely occlude functional coupling between neighbouring astrocytes (20). Second, to broadly target astrocyte function we used a calcium extruder pump (hPMCA2/b, a.k.a. CalEx) that has been shown to clamp astrocyte calcium at minimal levels, effectively silencing these cells (49,50). All viral constructs specifically targeted astrocytes with GfaABC1D promoter and were compared to a control virus expressing eGFP in astrocytes (**Figure 4B**). Initially, we screened for changes in anxiety-like behaviors using elevated plus maze and report no impact of lateral amygdala-specific astrocyte manipulation on the ratio of time spent in the open versus closed arms or in total distance traveled (**Figure S2B, C**). Next, using auditory discriminative fear conditioning paradigm, we found that learning was unaffected by astrocyte dysfunction (**Figure 4C** and **Table S1**). We also report that similar to ELS, lateral amygdala astrocytic dysfunction does not lead to hypersensitivity or hypervigilance to neutral

auditory cues (**Figure 4C, grey area).** During memory recall, however, we found that both
180 astrocyte manipulations enhanced fear responses to neutral cues, without affecting freezing to aversive cues (**Figure 4D**). This behavioural phenotype induced by astrocyte dysfunction alone mimics the effects of ELS on auditory fear discrimination, i.e. enhanced fear generalisation. Quantification of discrimination index revealed an impairment in discriminative fear memory in both dnCx43 and CalEx conditions, compared to viral control (**Figure 4E**). This effect is
185 dependent on the increase in freezing to the neutral cue with freezing responses to the aversive tone being unaltered by astrocytic dysfunction. These results directly implicate astrocytes in valence processing in the lateral amygdala and suggest a potential link between ELS and astrocyte dysfunction.

Next, we set out to determine whether astrocyte dysfunction in the lateral amygdala induced
190 similar synaptic plasticity deficits in cortico-amygdala circuits as observed in ELS. Again, using acute brain slice electrophysiology, we report an occlusion of LTP in both CalEx and dnCx43 conditions (**Figure 4F**).

Finally, in agreement with fear memory and synaptic plasticity changes, we found that astrocyte dysfunction directly influences neural excitability with increased c-Fos density
195 following fear conditioning in both CalEx and dnCx43 compared to control virus (**Figures 4G,H** and **S2D-F**). Taken together, these data highlight astrocytes as critical regulators of synaptic plasticity, neural excitability, and of discriminative fear memory.

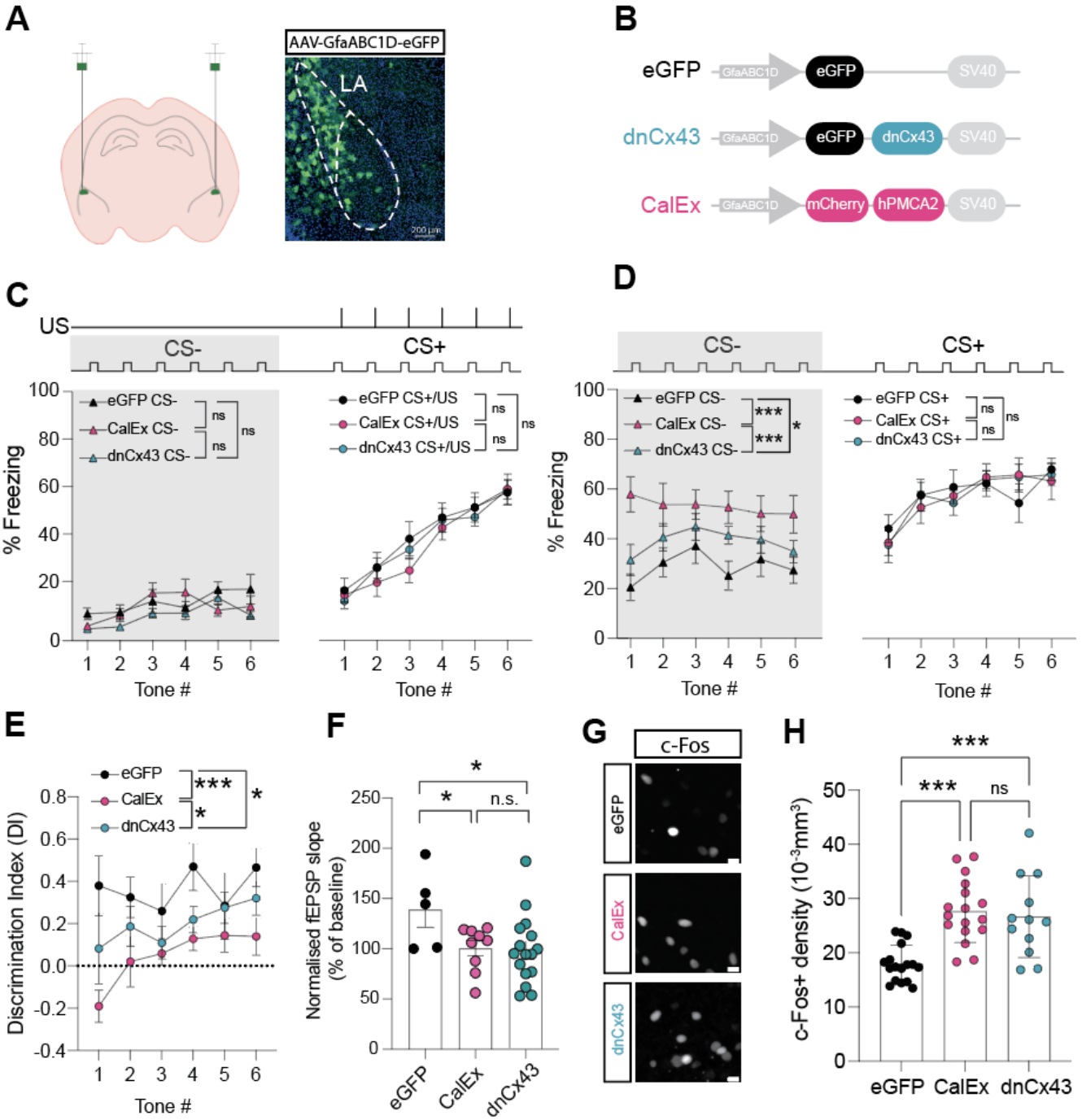

200 **<u>Figure 4. Astrocyte dysfunction mimics the effects of ELS on behaviour, synapses, and neural excitability.</u>**

(A) Representative image showing localisation of viral vector in lateral amygdala. **(B)** Viral constructs used to manipulate astrocyte function. **(C)** Astrocyte dysfunction did not affect % Freezing to neutral and

aversive auditory cues during learning. eGFP N=12, CalEx N=11, dnCx43 N=17 mice. **(D)** % time freezing during presentation of neutral auditory cue (CS-) was increased with astrocyte dysfunction (eGFP vs CalEx: p<0.0001; eGFP vs dnCx43: p=0.029; CalEx vs dnCx43: p=0.0005) with no impact on % Freezing to aversive cue (CS+). eGFP N=12, CalEx N=11, dnCx43 N=17 mice. **(E)** Discrimination Indexes were impaired by astrocyte dysfunction. eGFP vs CalEx: p<0.0001; eGFP vs dnCx43: p=0.013; CalEx vs dnCx43: p=0.03. eGFP N=12, CalEx N=11, dnCx43 N=17 mice. **(F)** Astrocyte dysfunction occluded the induction of LTP. eGFP vs CalEx: p=0.04; eGFP vs dnCx43: p=0.02; CalEx vs dnCx43: p=0.88. eGFP N=5, CalEx N=9, dnCx43 N=16. **(G)** Representative c-Fos staining in the lateral amygdala in control (eGFP), CalEx, and dnCx43 conditions 90 minutes after conditioning. Scale bars = 10μm. **(H)** c-Fos positive cell density was increased with astrocyte dysfunction. eGFP vs CalEx: p<0.0001; eGFP vs dnCx43: p=0.0005; CalEx vs dnCx43: p=0.88. eGFP n=17 slices N=5 mice, CalEx n=17 slices N=5 mice, dnCx43 n=12 slices N=5 mice. See Table S1 for detailed statistical summaries.

Discussion

In this study, we investigated the potential roles of astrocytes in cellular and behavioral dysfunctions associated with ELS. Using a rodent model of ELS that employs maternal separation and limited bedding, we report increased blood glucocorticoid levels associated with heightened anxiety-like behaviors. These endocrine and behavioural changes were accompanied by impaired discriminative fear memory in an amygdala-dependent auditory discrimination task. More precisely, we observed that ELS mice displayed increased fear responses to neutral cues with no change in freezing responses to aversive stimuli. These behavioral changes were further associated with alterations on the cellular scale including synaptic plasticity and neuronal excitability. Investigating contributions of non-neuronal cells, we found robust changes in lateral amygdala astrocytes following ELS comprising increased glucocorticoid receptor translocation to the nucleus and decreased expression of key astrocyte network proteins. To test the potential role of astrocyte dysfunction and how this might influence stress-induced behavioural changes, we genetically targeted lateral amygdala

astrocytes using a viral approach. Astrocyte dysfunction alone, we found, replicated the effects of stress on behavior, synapses, and excitability. Astrocytes have long been shown to be critical for memory formation, with the vast majority of studies reporting that astrocyte dysfunction impairs memory across various brain regions (30,47,49,52). Here we show that astrocyte dysfunction in the lateral amygdala effectively impairs discriminative fear memory evidenced by fear generalisation, *i.e.* the inappropriate expression of fear towards stimuli of neutral valence. These data reveal that astrocytes are critical for the appropriate behavioral responses to emotionally salient cues and provide evidence supporting the recently proposed contextual guidance theory of astrocyte function in the brain (51).

Using an ELS paradigm that coincides with peak astrocyte postnatal development (55,56), we found a latent increase in circulating glucocorticoids after ELS with peak levels appearing during late adolescence and subsiding towards adulthood. This transient effect may contribute to the enhanced susceptibility to stress observed during adolescence (57,58). Increased levels of blood glucocorticoids had a direct impact on astrocytes with increased translocation of GR from the cytosol to the nucleus of astrocytes following ELS, indicative of a higher levels of glucocorticoid signaling (46). While the effects of ELS on blood glucocorticoids was transient, this could have long-term consequences on protein expression levels resulting in changes in stress susceptibility. In humans, heightened levels of glucocorticoids in adolescents can be used to predict the occurrence of mood disorders many years later (58). The behavioural phenotype revealed by this work, i.e. ELS- and astrocyte dysfunction-induced fear generalisation, is a common trait observed in anxiety disorders that are commonly associated with fear generalisation(42). As such, these mechanisms give a starting point to further understand the neurobiological changes occurring in the brain in stress disorders.

Our work builds upon a growing literature that is interested in the potential roles of astrocytes in early-life stress (59–62). Our work identified specific astrocytic impairments induced by ELS and followed up with genetic manipulation of astrocyte function specifically in the lateral amygdala. These manipulations we found replicate cellular and fear generalisation phenotype observed following ELS, providing causal links between astrocyte dysfunction and impaired fear discrimination. We did not, however, observe an anxiety-like phenotype using elevated plus maze and open field, which could be interpreted as a lack of lateral amygdala astrocyte involvement in these discrete behaviors.

We find that both ELS and astrocyte dysfunction both enhance neuronal excitability, assessed by local c-Fos staining in the lateral amygdala following auditory discriminative fear conditioning. One interpretation of these data is that astrocytes might tune engram formation, with astrocyte dysfunction, genetically or after stress, increasing c-Fos expression resulting in a loss of specificity of the memory trace and generalisation of fear. Evidence of a cellular mechanism whereby increased c-Fos levels inversely correlate with memory accuracy have been recently shown in hippocampal circuits (45). In addition, astrocyte-engram neuron interactions have recently been identified (52) suggesting a potential participation of astrocytes in engram stabilisation. Our data are in line with previous reports that have demonstrated clear roles for astrocytes in memory formation and consolidation (31,53,54) and reveal that astrocytes participate in the neurobiological mechanisms by which stress influences emotional memory.

In sum, our data shed new light on the role of astrocytes as central regulators of amygdala-dependent behavior, synaptic function, and excitability. In addition, our work strongly suggests an astrocytic contribution to stress-induced behavioural and cellular impairments,

supporting the notion that astrocytic modifications are not simply downstream of neuronal dysfunction. These ideas are forcing a change in perception of how brain disorders develop, moving away from a neuro-centric cascade and placing astrocytes in the spotlight (51,64–68).

280 Taken together, these data support the hypothesis that astrocytes are key to execute the appropriate behavioral response to emotionally salient cues and highlight astrocytes as potential therapeutic targets for stress-related psychiatric disorders.

Acknowledgements

We thank Rosemary Bagot (McGill University) for critical input at the beginning of this study, Thierry Alquier and Stephanie Fulton (Université de Montréal) for their input throughout, Aurélie Cleret-Buhot (CRCHUM cellular imaging core) for microscopy training, and the staff of the animal facility at the CRCHUM. This work was funded by Canadian Institutes of Health Research Project Grant (478629), NSERC Discovery Grant (RGPIN-2021-03211), Fonds de Recherche du Québec – Santé (FRQS; 296562 & 309889), Brain and Behavior Research Foundation Young Investigator award (NARSAD; 28589), CHUM Foundation, Fondation Courtois, and the Réseau Québécois sur le Suicide les troubles de l'humeur et les troubles Associées (RQSHA) grant to C.M-R. I.I.A. and B.R. were both supported by a Canada Graduate Scholarship Master's awards, and Recruitment Fellowships from Neuroscience Dept. Université de Montréal. C.M-R. was supported by a Junior 1 Chercheur-Boursier salary award from FRQS.

Author Contributions

M.G. I.I.A., L.R.D-H, and C.M-R designed the study. M.G., I.I.A., O.G., J.L-A, J.V. and C.M-R. carried out behavioral experiments, analysing the subsequent data. M.G. and L.R.D-H. carried out immunostaining and analysis of subsequent data. L.R.D-H, M.D., B.R. took blood samples and performed ELISA experiments. M.G., L.R.D-H., O.G., and A.B. carried out injection of viral vectors. M.G. and A.B. carried out electrophysiological experiments and analysis of subsequent data. S.P. maintained and generated mouse colonies. M.G. L.R.D-H, A.B., and

C.M-R wrote the manuscript. All authors contributed to ELS paradigm and approved the final version of the manuscript.

Methods

Animals

All experiments were performed in accordance with the guidelines for maintenance and care of animals of the Canadian Council on Animal Care (CCAC) and approved by the Institutional Committee for the Protection of Animals (CIPA) at the Centre Hospitalier de l'Université de Montréal. Both male and female C57BL/6J mice (Jax #000664) were used in the study, housed on a 12hr:12hr light:dark cycle (lights on at 06:30) with *ad libitum* access to food and water.

Early Life Stress protocol

ELS was performed as previously described (6).C57BL/6J pups were separated from their mothers for 4-hours per day (ZT2-ZT6) for 7 days between ages P10 and P17. During separation pups and mothers were placed into new cages with 60% less bedding. Bedding was weighed on P10 and divided 33% into each cage (home cage, pup separation cage, and mother separation cage). Separated pups and mothers had *ad libitum* access to food and water and pup cages were placed on a water heating pad maintained at 34 degrees Celsius. After the final day of separation (P17) bedding was returned to the original amount and pups were housed with their mothers until weaning at P21.

Behavioral assays

Auditory Discriminative Fear Conditioning

Mice between ages P45-70 were used. Four days prior to behavioral testing mice were single housed in individual cages. Two days later mice were handled for approximately 10 minutes by

hand and mobilisation tube. On the first day of ADFC, single housed mice were left for 1 hour in behavioral room to habituate prior to the start of the conditioning assay.

Conditioning: Mice were first exposed to a neutral stimulus (CS-; white noise, 20s) repeated six times. After a two-minute interval mice were exposed to a tone which becomes the conditioned stimulus (CS+;12 kHz tone, 20s) as it co-terminates with a mild foot shock (Unconditioned stimulus (US); 0.5mA, 2s) delivered in the last two seconds of tone presentation (repeated six times). Conditioning was carried out in chamber with checkered walls that was cleaned with 70% ethanol between animals.

Memory recall: 24 hours after conditioning mice were exposed to CS- and CS+ (counterbalanced) in a novel environment characterised by stripped walls and a white floor covering, cleaned with 0.5% hydroperoxide between animals. Fear learning was quantified by the percentage of time spent freezing to CS- and CS+/US during the conditioning phase. Fear memory was quantified by the percentage time freezing to CS- or CS+ following presentation in the memory-recall phase. A discrimination index was calculated comparing fear responses to CS+ and CS- using the following formula;

$$Discrimination\ Index\ (DI) = \frac{(CS^{+}Freezing) - (CS^{-}Freezing)}{(CS^{+}\ Freezing) + (CS^{-}Freezing)}$$

Open Field Task

This task comprised of a total of 5 minutes and during that time the mice were left to freely explore the OFT apparatus, a white plexiglass box measuring 38x38 cm. During the task, mice were filmed, and the time spent in distinct parts of the box *i.e.* centre and periphery were quantified using AnyMaze software (Stoelting). The total time spent in the center was used as a quantification of anxiety-like behavior, where more time in the center represented less

anxiety-like behavior and the total distance travelled was measured to quantify locomotor changes.

355 *Elevated Plus Maze*

This task comprised of a total of 5 minutes during which mice were removed from their cages and placed at the centre of the four arms of the maze, facing an open arm. Mice were video recorded, and these videos were analysed using Anymaze software (Stoelting) which quantified the time spent (s) in closed arms or open arms during the 5min testing period.

360 Anxiety-like behavior was quantified by ratio of time spent in open vs closed arms.

Acute brain slice preparation

Coronal slices containing lateral amygdala were obtained from mice between P45-70. Animals were anesthetized with isoflurane and the brain was rapidly excised and placed in ice-cold

365 choline-based cutting solution saturated with 95% O_2 and 5% CO_2 containing the following (in mM): 120 choline chloride, 3 KCl, 1.25 NaH_2PO_4, 26 $NaHCO_3$, 8 $MgCl_2$, 20 glucose, pH 7.2 and 295 mOsmol. Slices (300 µm thick) were cut on a vibratome (Leica VT1200, Nussloch, Germany). Slices were transferred to oxygenated artificial CSF (ACSF) at 32 ± 0.5°C for 30 min containing the following (in mM): 130 NaCl, 2.5 KCl, 1.25 NaH_2PO_4, 26 $NaHCO_3$, 10 glucose,

370 1.3 $MgCl_2$, 2 $CaCl_2$, pH 7.3–7.4 and 300-305 mOsmol, then allowed to recover for at least 30 min before recordings in oxygenated ACSF at room temperature (RT). For experiments, the slices were transferred to a recording chamber where they were perfused (2 ml/min) with ACSF at 32ºC for the course of the experiment. Slices were used for a maximum of 6 hr after cutting.

375 **Electrophysiology**

Extracellular field excitatory postsynaptic potentials (fEPSPs) were recorded in current clamp mode with a pipette filled with ACSF placed in the lateral part of the amygdala. Monosynaptic EPSPs were elicited by stimulation of cortical afferences with a tungsten concentric bipolar electrode (World Precision Instruments). LTP was induced using a theta burst stimulation (TBS)
380 protocol consisting of 4 pulses at 100 Hz repeated at 5 Hz intervals for 10 seconds. Signals were amplified using a Multiclamp 700B amplifier (Molecular Devices) and digitized using the Digidata 1440 (Molecular Devices). Data were recorded (pClamp 10.2, Molecular Devices) for offline analysis. The magnitude of LTP was quantified by normalizing and averaging the slope of fEPSPs following LTP induction relative to the last 5 min of baseline.

385

Stereotaxic surgery and AAV delivery

P25-35 mice were given a subcutaneous (*s.c.*) injection of Carprofen (20 mg/kg) 1h prior surgery. Animals were then deeply anesthetised (2% isoflurane) before placing them into a stereotaxic frame (Kopf instruments). Surgical site was infiltrated with bupivacaine/lidocaine (2mg/kg *sc.*) 15
390 min prior surgery. Biliteral injections of the following viral constructs produced at the Canadian Neurophotonics Viral Vector Core: AAV2/5-gfaABC1D-eGFP (1.2-1.5x10^{11-12} GC/ml), AAV2/5-gfaABC1D-dnCx43-eGFP (1.2-1.7x10^{12} GC/ml) and AAV2/5-gfaABC1D-hPMCAw/b-mCherry (1.2x10^{12}) were delivered to the LA (coordinates relative to bregma: -1.4 mm AP, ± 3.4 mm ML and -5 mm DV) of mice of either sex. Viral solutions were injected at a rate of 200 nL/min for a
395 total volume of 650 nL per hemisphere using a 10 µl Hamilton syringe (Harvard apparatus) and a microinjection syringe pump (UMP3T-2 World Precision Instruments). Animals received 250 µL of saline for post-surgery hydration.

Brain processing.

400 Mice were anaesthetised in an enclosed chamber filled with isoflurane (5% for induction, 3-4% for maintenance, v/v) until loss of toe pinch reflex. A transcardial perfusion was used to ensure uniform preservation of tissue and brains were fixed in 4 % paraformaldehyde (PFA) for 24 hours at 4 degrees Celsius. The fixed brains were then placed in falcon tubes containing 30% sucrose solution for a minimum of two days. Brains were embedded in optimal cutting

405 temperature (OCT) compound and flash frozen in 2-methylbutane between -40 and -50 degrees Celsius and then stored at -80 until cryosectioning. Brains were cut at 30um thickness at -20 degrees Celsius using a Leica CM3050S Cryostat. Slices were stored in cryoprotector solution at 4 degrees Celsius until immunohistochemistry.

For c-fos labeling experiments, mice were anaesthetised and then perfused 90 minutes after

410 the end of fear conditioning. The whole lateral amygdala was sectioned in 30um thick brain slices and every fourth brain slice was selected for immunohistochemistry.

Immunohistochemistry.

Free floating brain slices were washed 3 times in 1X PBS for 15 minutes to remove

415 cryoprotector solution. Slices were permeabilised in block-perm solution (3% Bovine-Serum-Albumin, 0.5% Triton$^{10\%}$ in PBS) for a duration of 1 hour. Slices were incubated with antibodies for 24 hours at 4 degrees Celsius. Slices were incubated with primary antibodies; [Rabbit] anti-S100ß (1:1000, Abcam, ab52642), [Mouse] anti-glucocorticoid receptor (1:500, ThermoFisher, MA1-510), [Chicken] anti-GFAP (1:1000, ThermoFisher, PA1-10004), [mouse] anti-Cx43

420 (1:1000 ThermoFisher, 3D8A5), [Rabbit] Anti-GLT-1 (EAAT2) (1:1000, NovusBio, NBP1-

20136) and), [Rabbit] Anti-c-Fos (1:2000, Synaptic Systems, Cat.No. 226008). After primary antibody incubation slices were washed 3 times in 1X PBS for 15 minutes to remove non-specific binding. Slices were incubated with secondary antibodies in a DAPI solution (1:10000) at RT in aluminium foil for 1 hour. Slices were incubated with secondary antibodies; [goat] anti-rabbit Alexa 488 (1:1000, Jackson Immuno Research, 111-545-144), [goat] anti-mouse Alexa 647 (1:1000, ThermoFisher, A32728), [goat] anti-chicken Alexa 568 (1:1000, ThermoFisher, A11041). After secondary antibody incubation slices were washed again 3 times in 1X PBS for 15 minutes before being mounted onto Fisherbrand microscope slides using ProLong™ Glass Antifade mountant (P36982).

Microscopy

Slices were imaged using a Leica TCS SP5 laser scanning confocal microscope with oil immersion Plan-Apochromat 63x objective 1.4 NA, or using a Zeiss Observer Z1 spinning disk confocal microscope/TIRF with a 20x objective 1.8 NA. 16-bit images of 246 x 246 um areas were acquired at 400Hz (frame size (x*y); 1024 x 1024, pixel size; 250nm). 25-30um z-stacks were acquired with a step size of 0.5um. 15um max intensity z-projections of the lateral amygdala were analysed using Image-J (Fiji) to obtain A.U fluorescence intensity measures of secondary antibodies attached to primaries with specificity to epitopes; GFAP, Cx43, GLT-1, and GR. We applied a fluorescence threshold for GFAP, Cx43 and GLT-1 fluorescence and measured integrated density A.U (thresholds; Mean, Otsu, Otsu respectively). For nuclear and cytosolic Glucocorticoid Receptor measures, astrocyte (s100b+) DAPI nuclei were thresholded and used as ROIs for nuclear measures of GR fluorescence ($S100b^{+}$ + $DAPI^{+}$). The same nuclear DAPI ROI was cleared from the previously thresholded s100b regions to obtain

cytosolic astrocytic GR (S100b$^+$ - DAPI$^+$). Integrated density A.U of GR fluorescence was used
445 to calculate Nuclear:Cytosolic GR ratios.

For c-Fos cell counting in the lateral amygdala, 16-bit images containing the lateral and basal amygdala nuclei were acquired. 20-30 z-stacks were acquired with a step size of 1um. For c-Fos particle counting analysis, a region of interest was used to isolate the lateral amygdala and then 8-bit z-stacks of the c-Fos channel were analysed semi-automatically by using the FIJI
450 plugin Quanty-cfos (69). In brief, a threshold for area and fluorescence intensity was set manually to identify ROIs around all c-Fos positive nuclei. These ROIs were then manually inspected to remove false positives and negatives found by the plug-in. c-Fos particle counts were then normalized by the volume of the z-stack to calculate the c-Fos density. In order the calculate the volume, the area of the lateral amygdala was multiplied by the number of z-
455 stacks.

Blood Collection & Corticosterone analysis

Trunk blood was collected via decapitation at ZT2 (08:30). To minimise handling induced elevations in corticosterone mice were housed with clear plastic tubes used to move individual
460 mice intoan enclosed chamber filled with 5% isoflurane for 2 minutes. Mice were placed in enclosed Isoflurane until loss of toe pinch reflect (maximum elapsed time of 2 minutes). Mice were decapitated and trunk blood was collected into BD 365963 Microtainer® Capillary Blood Collection Tubes and placed onto Ice. Blood was centrifuged for 5 minutes at 4 degrees Celsius at 5000rpm. Serum was aliquoted and stored at -80 degrees Celsius. Corticosterone
465 measurements were obtained using an ENZO ELISA kit (ADI-900-097).

Statistical analyses

Results are presented as mean ±S.E.M. Data with one variable were analyzed with the two-tailed Student's *t* test or Mann-Whitney test. Data with more than two conditions were first screened for a Gaussian distribution with Kolmogorov-Smirnov test followed by analysis either with one-way/repeated measures ANOVA or Kruskal-Wallis/Friedman test when needed and Tukey's multiple-comparison parametric *post hoc* test (data with Gaussian distribution) or by a Dunn`s multiple-comparison non-parametric *post hoc* test (data with non-Gaussian distribution). Auditory discriminative fear conditioning data was analysed using a two-way ANOVA with appropriate post-hoc tests. Open field and elevated plus maze data analysed using one-way ANOVA with appropriate post hoc tests. Graphic significance levels were *, $p < 0.05$; **, $p < 0.01$ and ***, $p < 0.001$. All data were analyzed using GraphPad Prism software (Version 9, GraphPad, USA).

Data availability

The datasets that support the findings of this study are available from the corresponding author upon request.

References

1. Walker CD, Bath KG, Joels M, Korosi A, Larauche M, Lucassen PJ, *et al.* (2017): Chronic early life stress induced by limited bedding and nesting (LBN) material in rodents: critical considerations of methodology, outcomes and translational potential. *Stress* 20: 421–448.
2. Joëls M, Baram TZ (2009): The neuro-symphony of stress. *Nat Rev Neurosci* 10: 459–466.
3. Lopez J, Bagot RC (2021): Defining Valid Chronic Stress Models for Depression With Female Rodents. *Biol Psychiatry* 90: 226–235.
4. O'Donnell KJ, Meaney MJ (2020, May 7): Epigenetics, Development, and Psychopathology. *Annual Review of Clinical Psychology*, vol. 16. Annual Reviews Inc., pp 327–350.
5. Meaney MJ (2001): Maternal Care, Gene Expression, and the Transmission of Individual Differences in Stress Reactivity Across Generations. *Annu Rev Neurosci* 24: 1161–1192.
6. Peña CJ, Kronman HG, Walker DM, Cates HM, Bagot RC, Purushothaman I, *et al.* (2017): Early life stress confers lifelong stress susceptibility in mice via ventral tegmental area OTX2. *Science (1979)* 356: 1185–1188.
7. Peña CJ, Nestler EJ, Bagot RC (2019): Environmental Programming of Susceptibility and Resilience to Stress in Adulthood in Male Mice. *Front Behav Neurosci* 13: 40.
8. Lesuis SL, Weggen S, Baches S, Lucassen PJ, Krugers HJ (2018): Targeting glucocorticoid receptors prevents the effects of early life stress on amyloid pathology and cognitive performance in APP/PS1 mice. *Transl Psychiatry* 8: 53.
9. Lesuis SL, Lucassen PJ, Krugers HJ (2019): Early life stress impairs fear memory and synaptic plasticity; a potential role for GluN2B. *Neuropharmacology* 149: 195–203.
10. Ramkumar R, Edge-Partington M, Terstege DJ, Adigun K, Ren Y, Khan NS, *et al.* (2024): Long-term impact of early life stress on serotonin connectivity. *Biol Psychiatry* 0. https://doi.org/10.1016/j.biopsych.2024.01.024
11. Lupien SJ, McEwen BS, Gunnar MR, Heim C (2009): Effects of stress throughout the lifespan on the brain, behaviour and cognition. *Nat Rev Neurosci* 10: 434–445.
12. Bains JS, Cusulin JIW, Inoue W (2015): Stress-related synaptic plasticity in the hypothalamus. *Nat Rev Neurosci* 16: 377–388.
13. Senst L, Baimoukhametova D, Sterley T-L, Bains JS (2016): Sexually dimorphic neuronal responses to social isolation. *Elife* 5. https://doi.org/10.7554/eLife.18726
14. Wamsteeker Cusulin JI, Füzesi T, Inoue W, Bains JS (2013): Glucocorticoid feedback uncovers retrograde opioid signaling at hypothalamic synapses. *Nat Neurosci* 16: 596–604.
15. Füzesi T, Daviu N, Wamsteeker Cusulin JI, Bonin RP, Bains JS (2016): Hypothalamic CRH neurons orchestrate complex behaviours after stress. *Nat Commun* 7: 11937.
16. Daviu N, Füzesi T, Rosenegger DG, Rasiah NP, Sterley TL, Peringod G, Bains JS (2020): Paraventricular nucleus CRH neurons encode stress controllability and regulate defensive behavior selection. *Nat Neurosci* 23: 398–410.
17. Guadagno A, Wong TP, Walker CD (2018): Morphological and functional changes in the preweaning basolateral amygdala induced by early chronic stress associate with anxiety and fear behavior in adult male, but not female rats. *Prog Neuropsychopharmacol Biol Psychiatry* 81: 25–37.

18. Guadagno A, Belliveau C, Mechawar N, Walker C-D (2021): Effects of Early Life Stress on the Developing Basolateral Amygdala-Prefrontal Cortex Circuit: The Emerging Role of Local Inhibition and Perineuronal Nets. *Front Hum Neurosci* 15. https://doi.org/10.3389/fnhum.2021.669120
19. Guadagno A, Kang MS, Devenyi GA, Mathieu AP, Rosa-Neto P, Chakravarty M, Walker CD (2018): Reduced resting-state functional connectivity of the basolateral amygdala to the medial prefrontal cortex in preweaning rats exposed to chronic early-life stress. *Brain Struct Funct* 223: 3711–3729.
20. Murphy-Royal C, Johnston AD, Boyce AKJ, Diaz-Castro B, Institoris A, Peringod G, *et al.* (2020): Stress gates an astrocytic energy reservoir to impair synaptic plasticity. *Nat Commun* 11: 2014.
21. Lau BK, Murphy-Royal C, Kaur M, Qiao M, Bains JS, Gordon GR, Borgland SL (2021): Obesity-induced astrocyte dysfunction impairs heterosynaptic plasticity in the orbitofrontal cortex. *Cell Rep* 36: 109563.
22. Henneberger C, Papouin T, Oliet SHR, Rusakov DA (2010): Long-term potentiation depends on release of D-serine from astrocytes. *Nature* 463: 232–6.
23. Papouin T, Dunphy JM, Tolman M, Dineley KT, Haydon PG (2017): Septal Cholinergic Neuromodulation Tunes the Astrocyte-Dependent Gating of Hippocampal NMDA Receptors to Wakefulness. *Neuron* 94: 840-854.e7.
24. Covelo A, Araque A (2018): Neuronal activity determines distinct gliotransmitter release from a single astrocyte. *Elife* 7. https://doi.org/10.7554/eLife.32237
25. Panatier A, Vallée J, Haber M, Murai KK, Lacaille J-C, Robitaille R (2011): Astrocytes are endogenous regulators of basal transmission at central synapses. *Cell* 146: 785–98.
26. Panatier A, Theodosis DT, Mothet J-P, Touquet B, Pollegioni L, Poulain DA, Oliet SHR (2006): Glia-Derived d-Serine Controls NMDA Receptor Activity and Synaptic Memory. *Cell* 125: 775–784.
27. Matos M, Bosson A, Riebe I, Reynell C, Vallée J, Laplante I, *et al.* (2018): Astrocytes detect and upregulate transmission at inhibitory synapses of somatostatin interneurons onto pyramidal cells. *Nat Commun* 9: 4254.
28. Nagai J, Yu X, Papouin T, Cheong E, Freeman MR, Monk KR, *et al.* (2021): Behaviorally consequential astrocytic regulation of neural circuits. *Neuron* 109: 576–596.
29. Wahis J, Baudon A, Althammer F, Kerspern D, Goyon S, Hagiwara D, *et al.* (2021): Astrocytes mediate the effect of oxytocin in the central amygdala on neuronal activity and affective states in rodents. *Nat Neurosci* 24: 529–541.
30. Robin LM, Oliveira da Cruz JF, Langlais VC, Martin-Fernandez M, Metna-Laurent M, Busquets-Garcia A, *et al.* (2018): Astroglial CB1 Receptors Determine Synaptic D-Serine Availability to Enable Recognition Memory. *Neuron* 98: 935-944.e5.
31. Martin-Fernandez M, Jamison S, Robin LM, Zhao Z, Martin ED, Aguilar J, *et al.* (2017): Synapse-specific astrocyte gating of amygdala-related behavior. *Nat Neurosci* 20: 1540–1548.
32. Yu X, Taylor AMMW, Nagai J, Golshani P, Evans CJ, Coppola G, Khakh BS (2018): Reducing Astrocyte Calcium Signaling In Vivo Alters Striatal Microcircuits and Causes Repetitive Behavior. *Neuron* 99: 1170-1187.e9.

33. Corkrum M, Covelo A, Lines J, Bellocchio L, Pisansky M, Loke K, *et al.* (2020): Dopamine-Evoked Synaptic Regulation in the Nucleus Accumbens Requires Astrocyte Activity. *Neuron* 105: 1036.
34. Nagai J, Rajbhandari AK, Gangwani MR, Hachisuka A, Coppola G, Masmanidis SC, *et al.* (2019): Hyperactivity with Disrupted Attention by Activation of an Astrocyte Synaptogenic Cue. *Cell* 177: 1280-1292.e20.
35. Doron A, Rubin A, Benmelech-Chovav A, Benaim N, Carmi T, Refaeli R, *et al.* (2022): Hippocampal astrocytes encode reward location. *Nature* 609: 772–778.
36. Mu Y, Bennett D V, Rubinov M, Narayan S, Yang C-T, Tanimoto M, *et al.* (2019): Glia Accumulate Evidence that Actions Are Futile and Suppress Unsuccessful Behavior. *Cell* 178: 27-43.e19.
37. Ressler KJ (2010): Amygdala Activity, Fear, and Anxiety: Modulation by Stress. *Biol Psychiatry* 67: 1117.
38. Cohen MM, Jing D, Yang RR, Tottenham N, Lee FS, Casey BJ (2013): Early-life stress has persistent effects on amygdala function and development in mice and humans. *Proc Natl Acad Sci U S A* 110: 18274–18278.
39. Roozendaal B, McEwen BS, Chattarji S (2009, May 13): Stress, memory and the amygdala. *Nature Reviews Neuroscience*, vol. 10. Nature Publishing Group, pp 423–433.
40. Kim W Bin, Cho JH (2017): Encoding of Discriminative Fear Memory by Input-Specific LTP in the Amygdala. *Neuron* 95: 1129-1146.e5.
41. Asok A, Kandel ER, Rayman JB (2019): The neurobiology of fear generalization. *Front Behav Neurosci* 12: 427950.
42. Dymond S, Dunsmoor JE, Vervliet B, Roche B, Hermans D (2015): Fear Generalization in Humans: Systematic Review and Implications for Anxiety Disorder Research. *Behav Ther* 46: 561–582.
43. Han JH, Kushner SA, Yiu AP, Hsiang HL, Buch T, Waisman A, *et al.* (2009): Selective erasure of a fear memory. *Science* 323: 1492–1496.
44. Rashid AJ, Yan C, Mercaldo V, Hsiang HL, Park S, Cole CJ, *et al.* (2016): Competition between engrams influences fear memory formation and recall. *Science* 353: 383–387.
45. Ramsaran AI, Wang Y, Golbabaei A, Aleshin S, de Snoo ML, Yeung BRA, *et al.* (2023): A shift in the mechanisms controlling hippocampal engram formation during brain maturation. *Science (1979)* 380: 543–551.
46. De Kloet ER, Joëls M, Holsboer F (2005): Stress and the brain: from adaptation to disease. *Nat Rev Neurosci* 6: 463–475.
47. Giaume C, Koulakoff A, Roux L, Holcman D, Rouach N (2010): Astroglial networks: a step further in neuroglial and gliovascular interactions. *Nat Rev Neurosci* 11: 87–99.
48. Murphy-Royal C, Dupuis JP, Varela JA, Panatier A, Pinson B, Baufreton J, *et al.* (2015): Surface diffusion of astrocytic glutamate transporters shapes synaptic transmission. *Nat Neurosci* 18: 219–26.
49. Institoris A, Vandal M, Peringod G, Catalano C, Tran CH, Yu X, *et al.* (2022): Astrocytes amplify neurovascular coupling to sustained activation of neocortex in awake mice. *Nature Communications 2022 13:1* 13: 1–17.

50. Yu X, Taylor AMW, Nagai J, Golshani P, Evans CJ, Coppola G, Khakh BS (2018): Reducing Astrocyte Calcium Signaling In Vivo Alters Striatal Microcircuits and Causes Repetitive Behavior. *Neuron* 99: 1170-1187.e9.
51. Murphy-Royal C, Ching SN, Papouin T (2023): A conceptual framework for astrocyte function. *Nat Neurosci* 26: 1848–1856.
52. Kim J, Sung Y, Park H, Choi D Il, Kim J, Lee H, *et al.* (2023): Astrocytic connection to engram neurons Increased after learning. *bioRxiv* 2023.01.25.525617.
53. Kol A, Adamsky A, Groysman M, Kreisel T, London M, Goshen I (2020): Astrocytes contribute to remote memory formation by modulating hippocampal–cortical communication during learning. *Nat Neurosci* 1–11.
54. Adamsky A, Kol A, Kreisel T, Doron A, Ozeri-Engelhard N, Melcer T, *et al.* (2018): Astrocytic Activation Generates De Novo Neuronal Potentiation and Memory Enhancement. *Cell* 174: 59-71.e14.
55. Rurak GM, Simard S, Freitas-Andrade M, Lacoste B, Charih F, Van Geel A, *et al.* (2022): Sex differences in developmental patterns of neocortical astroglia: A mouse translatome database. *Cell Rep* 38. https://doi.org/10.1016/J.CELREP.2022.110310
56. Farhy-Tselnicker I, Allen NJ (2018, May 1): Astrocytes, neurons, synapses: A tripartite view on cortical circuit development. *Neural Development*, vol. 13. BioMed Central Ltd., pp 1–12.
57. Sisk LM, Gee DG (2022): Stress and adolescence: Vulnerability and opportunity during a sensitive window of development. *Curr Opin Psychol* 44: 286.
58. Ellenbogen MA, Hodgins S, Linnen AM, Ostiguy CS (2011): Elevated daytime cortisol levels: A biomarker of subsequent major affective disorder? *J Affect Disord* 132: 265–269.
59. Vivi E, Di Benedetto B (2024): Brain stars take the lead during critical periods of early postnatal brain development: relevance of astrocytes in health and mental disorders. *Molecular Psychiatry 2024* 1–13.
60. Abbink MR, van Deijk ALF, Heine VM, Verheijen MH, Korosi A (2019, September 1): The involvement of astrocytes in early-life adversity induced programming of the brain. *GLIA*, vol. 67. John Wiley and Sons Inc., pp 1637–1653.
61. Gunn BG, Cunningham L, Cooper MA, Corteen NL, Seifi M, Swinny JD, *et al.* (2013): Dysfunctional astrocytic and synaptic regulation of hypothalamic glutamatergic transmission in a mouse model of early-life adversity: relevance to neurosteroids and programming of the stress response. *J Neurosci* 33: 19534–54.
62. Abbink MR, van Deijk ALF, Heine VM, Verheijen MH, Korosi A (2019): The involvement of astrocytes in early-life adversity induced programming of the brain. *Glia* 67: 1637–1653.
63. Bosson A, Paumier A, Boisseau S, Jacquier-Sarlin M, Buisson A, Albrieux M (2017): TRPA1 channels promote astrocytic Ca2+ hyperactivity and synaptic dysfunction mediated by oligomeric forms of amyloid-β peptide. *Mol Neurodegener* 12. https://doi.org/10.1186/S13024-017-0194-8
64. Vivi E, Di Benedetto B (2024): Brain stars take the lead during critical periods of early postnatal brain development: relevance of astrocytes in health and mental disorders. *Molecular Psychiatry 2024* 1–13.
65. Seifert G, Schilling K, Steinhäuser C (2006): Astrocyte dysfunction in neurological disorders: a molecular perspective. *Nature Reviews Neuroscience 2006 7:3* 7: 194–206.

66. Lee HG, Wheeler MA, Quintana FJ (2022): Function and therapeutic value of astrocytes in neurological diseases. *Nature Reviews Drug Discovery 2022 21:5* 21: 339–358.
67. Endo F, Kasai A, Soto JS, Yu X, Qu Z, Hashimoto H, *et al.* (2022): Molecular basis of astrocyte diversity and morphology across the CNS in health and disease. *Science* 378. https://doi.org/10.1126/SCIENCE.ADC9020
68. Khakh BS, Goldman SA (2023): Astrocytic contributions to Huntington's disease pathophysiology. *Ann N Y Acad Sci* 1522: 42–59.
69. Beretta CA, Liu S, Stegemann A, Gan Z, Wang L, Tan LL, Kuner R (2023): Quanty-cFOS, a Novel ImageJ/Fiji Algorithm for Automated Counting of Immunoreactive Cells in Tissue Sections. *Cells* 12. https://doi.org/10.3390/CELLS12050704

Figures

Early-life stress induces persistent astrocyte dysfunction resulting in fear generalisation

Guayasamin M., Depaauw-Holt L.R., Adedipe I.I., et al.

Figure 1

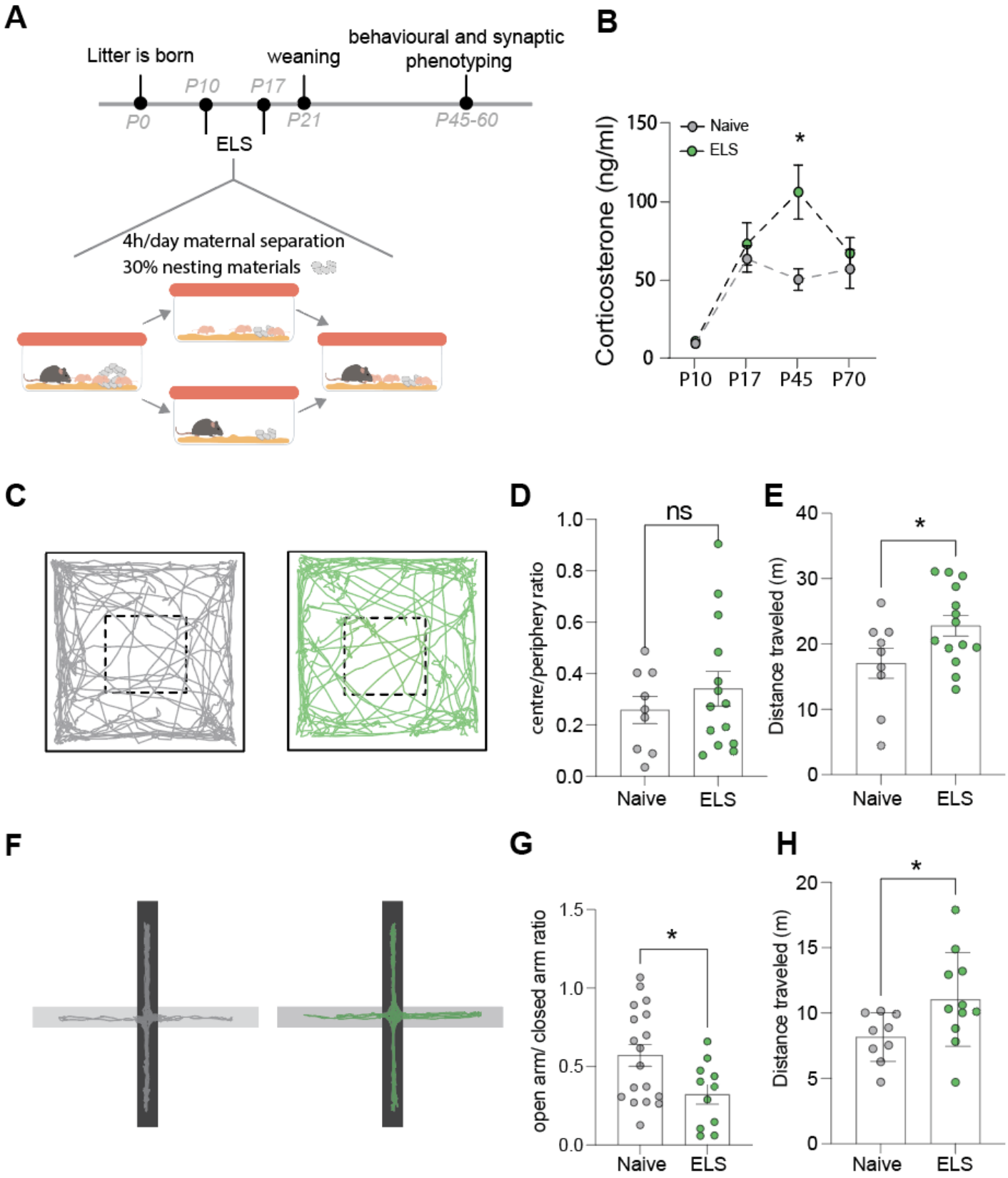
A
Litter is born
weaning
behavioural and synaptic phenotyping
P0
P10
P17
P21
P45-60
ELS
4h/day maternal separation
30% nesting materials
B
Corticosterone (ng/ml)
Naive
ELS
P10
P17
P45
P70
C
D
ns
centre/periphery ratio
Naive
ELS
E
Distance traveled (m)
Naive
ELS
F
G
open arm/ closed arm ratio
Naive
ELS
H
Distance traveled (m)
Naive
ELS

Figure 1. Effects of ELS on anxiety-like behavior.

(A) Timeline of ELS and behavioral assays. **(B)** Serum corticosterone levels are increased during
665 adolescence, following ELS. P=0.01, Naïve N=9, ELS N=11 mice. **(C)** Representative movement tracks of naive (grey) and ELS (green) mice in open field task. **(D)** No significant difference in centre/periphery ratio in open field following ELS. P=0.39, Naïve N=9, ELS N=14 mice. **(E)** Total distance travelled during open field test was increased in ELS mice. P=0.04, Naïve N=9, ELS N=14 mice. **(F)** Representative locomotor tracks in elevated plus maze in naïve and ELS mice, black segment represents closed arms
670 with grey arms representing open arms. **(G)** ELS mice had a reduced open/closed arm ratio. P=0.02, Naïve N=18, ELS N=11 mice. **(H)** Total distance travelled during elevated plus maze test was increased by ELS. P=0.02, Naïve N=9, ELS N=11 mice. See Table S1 for detailed statistical summaries.

Figure 2

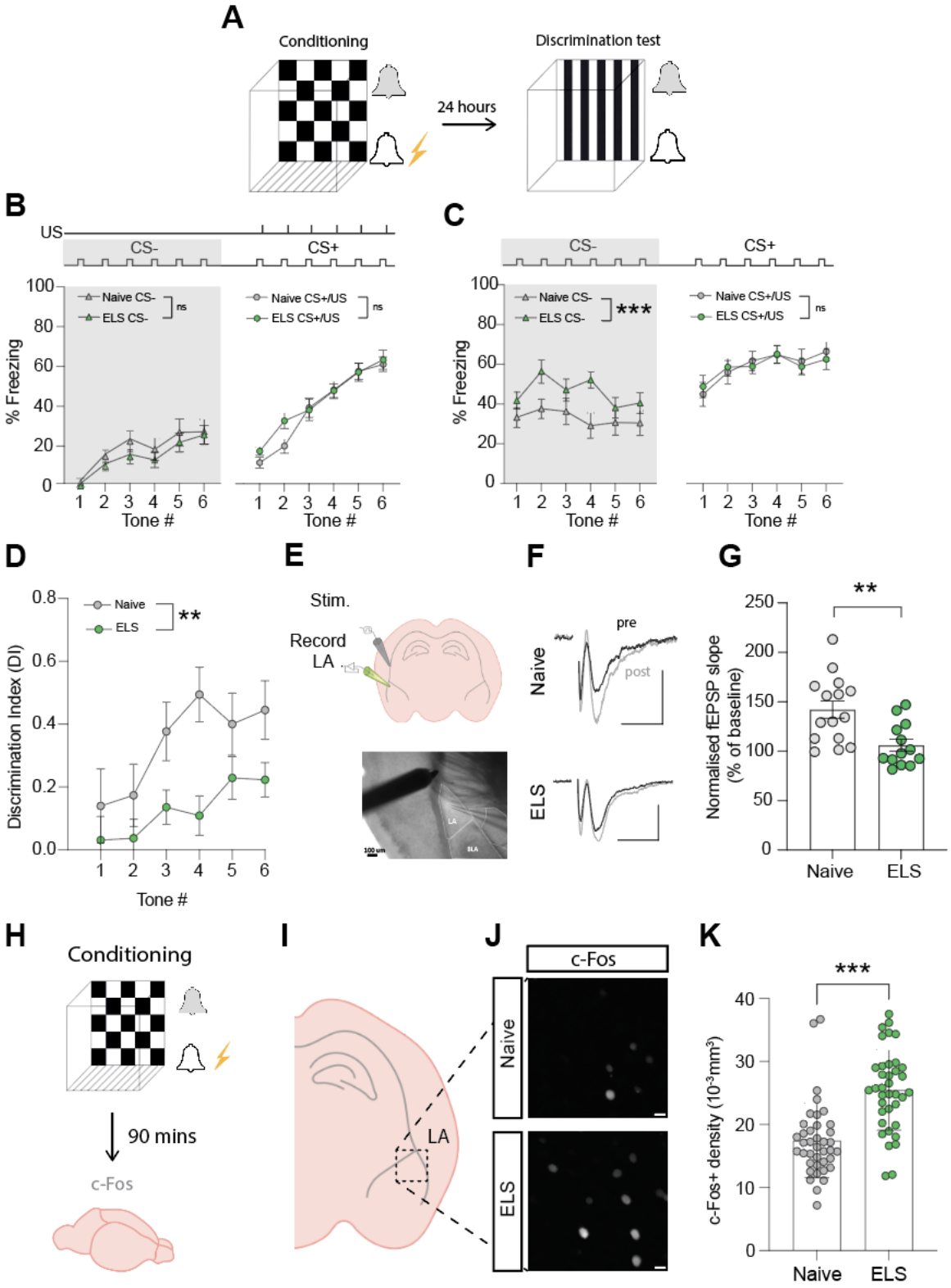
A
Conditioning
Discrimination test
24 hours
B
US
CS-
CS+
Naive CS-
ELS CS-
ns
Naive CS+/US
ELS CS+/US
ns
% Freezing
Tone #
C
CS-
CS+
Naive CS-
ELS CS-
***
Naive CS+/US
ELS CS+/US
ns
% Freezing
Tone #
D
Naive
ELS
**
Discrimination Index (DI)
Tone #
E
Stim.
Record LA
F
pre
post
Naive
ELS
G
**
Normalised fEPSP slope (% of baseline)
Naive
ELS
H
Conditioning
90 mins
c-Fos
I
LA
J
c-Fos
Naive
ELS
K
***
c-Fos+ density (10⁻³mm³)
Naive
ELS

Figure 2. ELS alters fear memory, synaptic plasticity, and neural excitability.

675 **(A)** Timeline of auditory discriminative fear conditioning paradigm. **(B)** ELS did not affect % Freezing to neutral and aversive auditory cues during learning. Naïve N=20, ELS N=17. **(C)** % time freezing during presentation of neutral auditory cue (CS-; p=0.0002) and aversive cue (CS+; p=0.99). Naïve N=20, ELS N=17. **(D)** Discrimination Index was impaired by ELS. P=0.004. Naïve N=20, ELS N=17. **(E)** Schematic representation of electrode placement in slice electrophysiology experiment (top) with DIC image

680 below. **(F)** Representative EPSP traces from naïve (top) and ELS (bottom) brain slices during baseline (black trace) and after LTP stimulation (grey trace). Scale bars = 0.5mV and 10ms. **(G)** LTP was impaired by ELS. P=0.002. Naïve N=15, ELS N=13. **(H)** Diagram of procedure for c-fos staining experiments. **(I)** Brain slices containing lateral amygdala (LA) were selected for c-Fos staining. **(J)** Region of interested extracted from full amygdala image. Scale bars = 10μm. **(K)** c-Fos positive cell density was increased by

685 ELS. P<0.0001. Naïve n=39 slices N=10 mice, ELS n=37 slices N=10mice. See Table S1 for detailed statistical summaries.

Figure 3

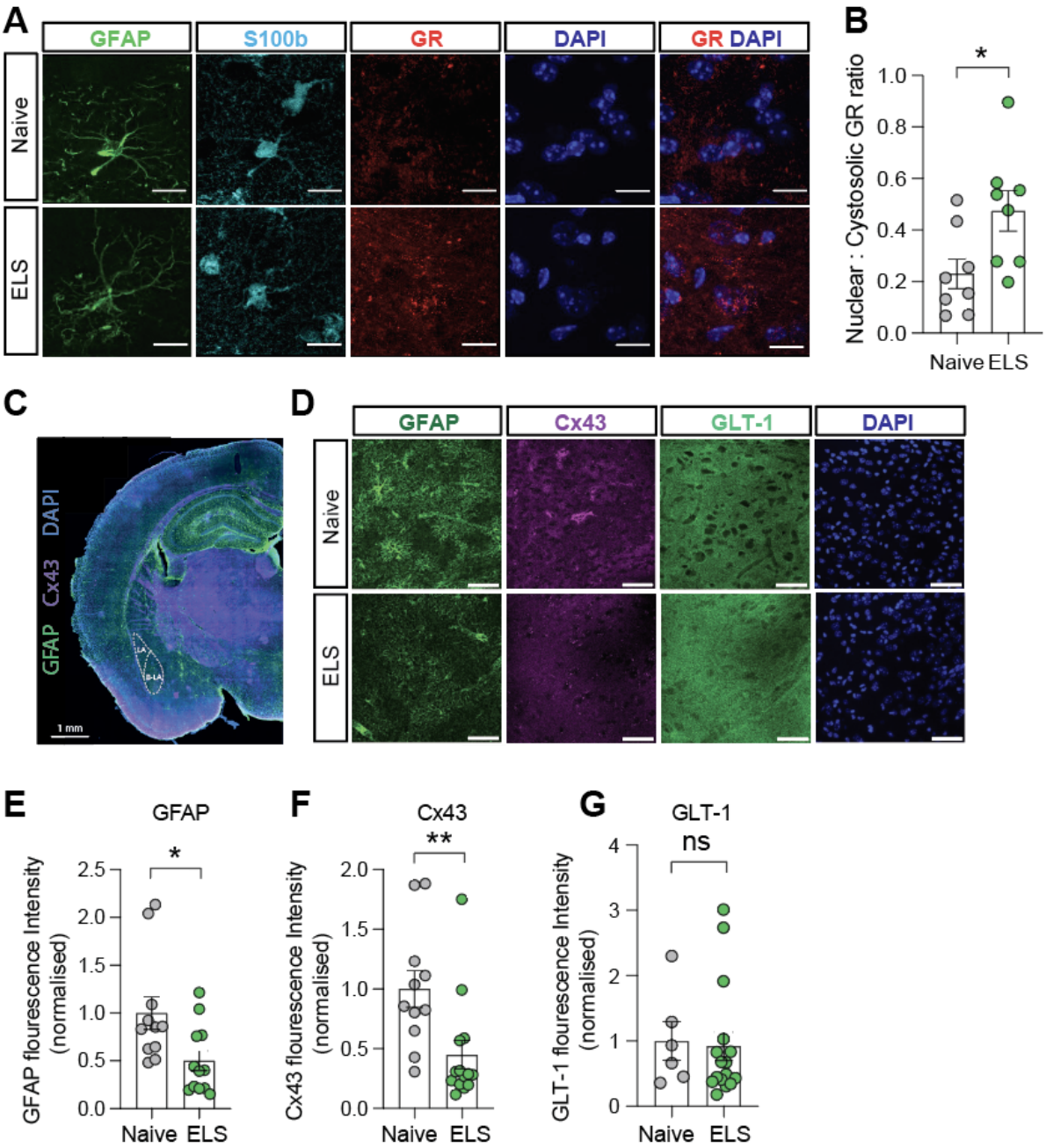
A
GFAP
S100b
GR
DAPI
GR DAPI
Naive
ELS
B
Nuclear : Cystosolic GR ratio
1.0
0.8
0.6
0.4
0.2
0.0
*
Naive ELS
C
DAPI
Cx43
GFAP
1 mm
D
GFAP
Cx43
GLT-1
DAPI
Naive
ELS
E
GFAP
GFAP flourescence Intensity (normalised)
2.5
2.0
1.5
1.0
0.5
0.0
*
Naive ELS
F
Cx43
Cx43 flourescence Intensity (normalised)
2.0
1.5
1.0
0.5
0.0
**
Naive ELS
G
GLT-1
ns
GLT-1 flourescence Intensity (normalised)
4
3
2
1
0
Naive ELS

690

Figure 3. Long-term astrocyte dysfunction after early-life stress.

(A) Representative immunostaining of GFAP, S100b, GR, DAPI, and GR/DAPI merge in Naïve and ELS conditions. Scale bars = 20μm **(B)** Nuclear/cystolic GR ratio in astrocytes was increased after ELS. P=0.026. Naïve N=8, ELS N=8. **(C)** Representative slide scan image of immunostaining for astrocyte
695 proteins GFAP and Cx43. **(D)** Representative immunostaining of GFAP, Cx43, GLT-1, and DAPI in naïve and ELS conditions. Scale bars = 50μm **(E)** GFAP staining was reduced in ELS mice. p=0.02, Naïve N=11, ELS N=12. **(F)** Cx43 staining was decreased in ELS mice. p=0.008. Naïve N=11, ELS=14. **(G)** GLT-1 expression was unchanged by ELS. P=0.8. Naïve N=6, ELS N=16. See Table S1 for detailed statistical summaries.

Figure 4

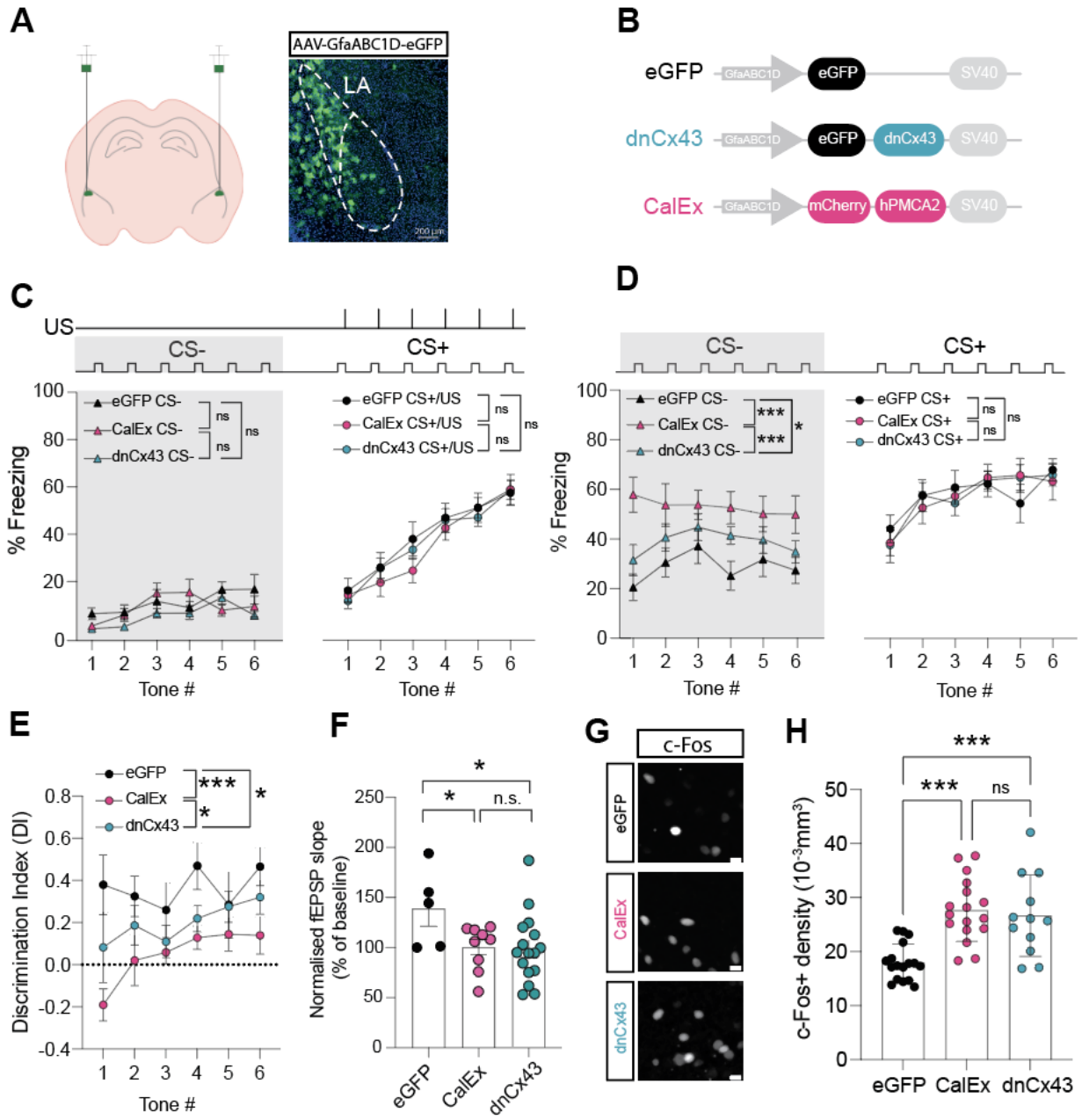
A
AAV-GfaABC1D-eGFP
LA
B
eGFP
GfaABC1D
eGFP
SV40
dnCx43
GfaABC1D
eGFP
dnCx43
SV40
CalEx
GfaABC1D
mCherry
hPMCA2
SV40
C
US
CS-
CS+
% Freezing
eGFP CS-
CalEx CS-
dnCx43 CS-
ns
eGFP CS+/US
CalEx CS+/US
dnCx43 CS+/US
Tone #
D
eGFP CS+
CalEx CS+
dnCx43 CS+
***
*
E
eGFP
CalEx
dnCx43
Discrimination Index (DI)
Tone #
F
Normalised fEPSP slope (% of baseline)
n.s.
eGFP
CalEx
dnCx43
G
c-Fos
eGFP
CalEx
dnCx43
H
c-Fos+ density (10⁻³mm³)
ns
eGFP
CalEx
dnCx43

700

Figure 4. Astrocyte dysfunction mimics the effects of ELS on behavior, synapses, and neural excitability.

705 **(A)** Representative image showing localisation of viral vector in lateral amygdala. **(B)** Viral constructs used to manipulate astrocyte function. **(C)** Astrocyte dysfunction did not affect % Freezing to neutral and aversive auditory cues during learning. eGFP N=12, CalEx N=11, dnCx43 N=17 mice. **(D)** % time freezing during presentation of neutral auditory cue (CS-) was increased with astrocyte dysfunction (eGFP vs CalEx: $p<0.0001$; eGFP vs dnCx43: $p=0.029$; CalEx vs dnCx43: $p=0.0005$) with no impact on % Freezing to

710 aversive cue (CS+). eGFP N=12, CalEx N=11, dnCx43 N=17 mice. **(E)** Discrimination Indexes were impaired by astrocyte dysfunction. eGFP vs CalEx: $p<0.0001$; eGFP vs dnCx43: $p=0.013$; CalEx vs dnCx43: $p=0.03$. eGFP N=12, CalEx N=11, dnCx43 N=17 mice. **(F)** Astrocyte dysfunction occluded the induction of LTP. eGFP vs CalEx: $p=0.04$; eGFP vs dnCx43: $p=0.02$; CalEx vs dnCx43: $p=0.88$. eGFP N=5, CalEx N=9, dnCx43 N=16. **(G)** Representative c-Fos staining in the lateral amygdala in control (eGFP), CalEx, and dnCx43

715 conditions. Scale bars = 10μm. **(H)** c-Fos positive cell density was increased with astrocyte dysfunction. eGFP vs CalEx: $p<0.0001$; eGFP vs dnCx43: $p=0.0005$; CalEx vs dnCx43: $p=0.88$. eGFP n=17 slices N=5 mice, CalEx n=17 slices N=5 mice, dnCx43 n=12 slices N=5 mice.

See Table S1 for detailed statistical summaries.

Supplementary Figure 1

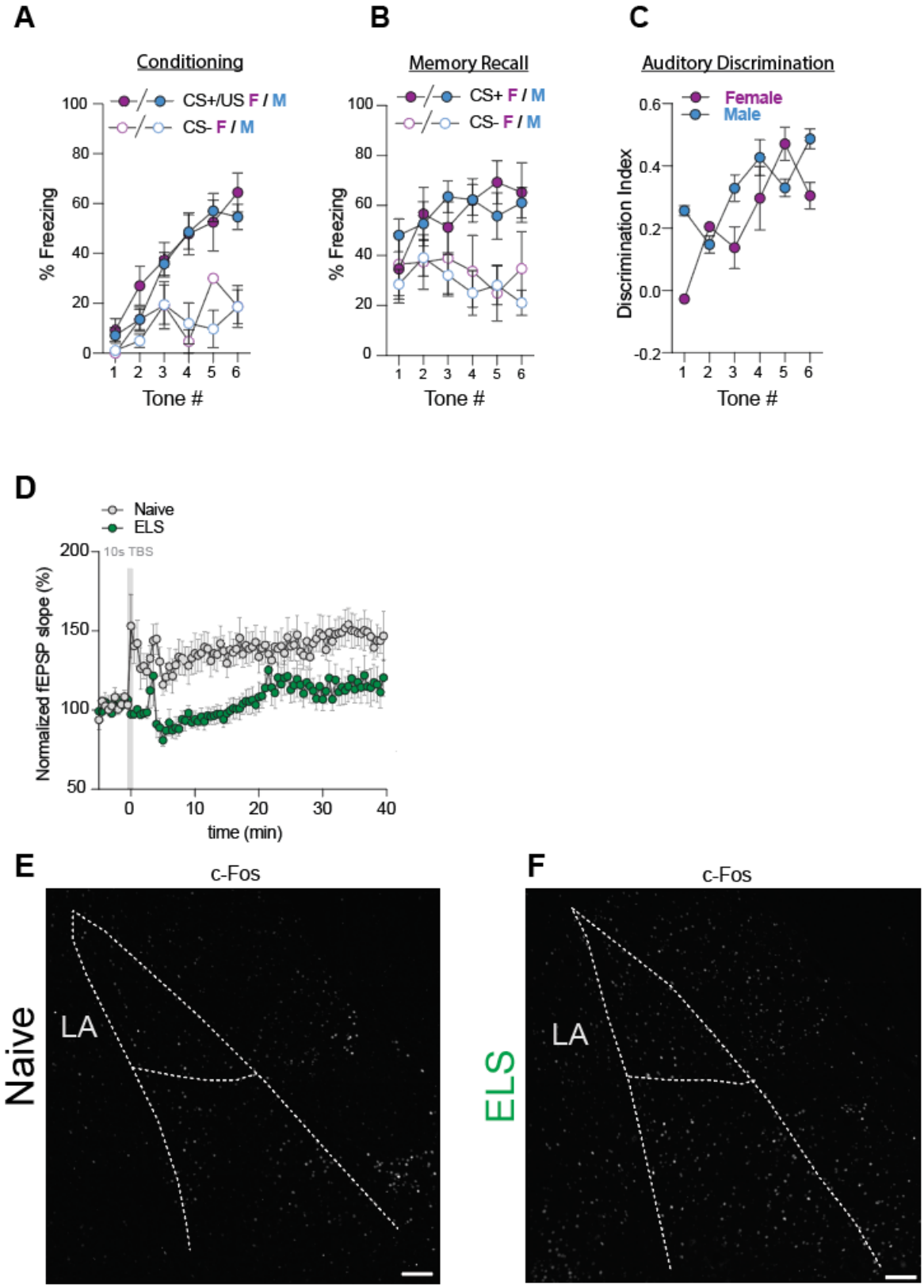

(A) Learning phase (conditioning) of auditory discriminative fear conditioning in male and female naïve
720 mice. Female N=7, Male N=8. **(B)** Memory recall in of CS+ and CS- in male and female naïve mice. Female N=7, Male N=8. **(C)** Auditory discrimination in male and female naïve mice. Female N=7, Male N=8. **(D)** Normalised fEPSP slope showing synaptic response before and after theta burst stimulation (grey vertical bar) in naïve and ELS mice. **(E)** Representative Z-stack projection of c-FOs staining in entire LA and BLA in naive. **(F)** Z-stack projection of c-FOs staining in entire LA and BLA in ELS. Scale
725 bars = 100μm. See Table S1 for detailed statistical comparisons.

Supplementary figure 2

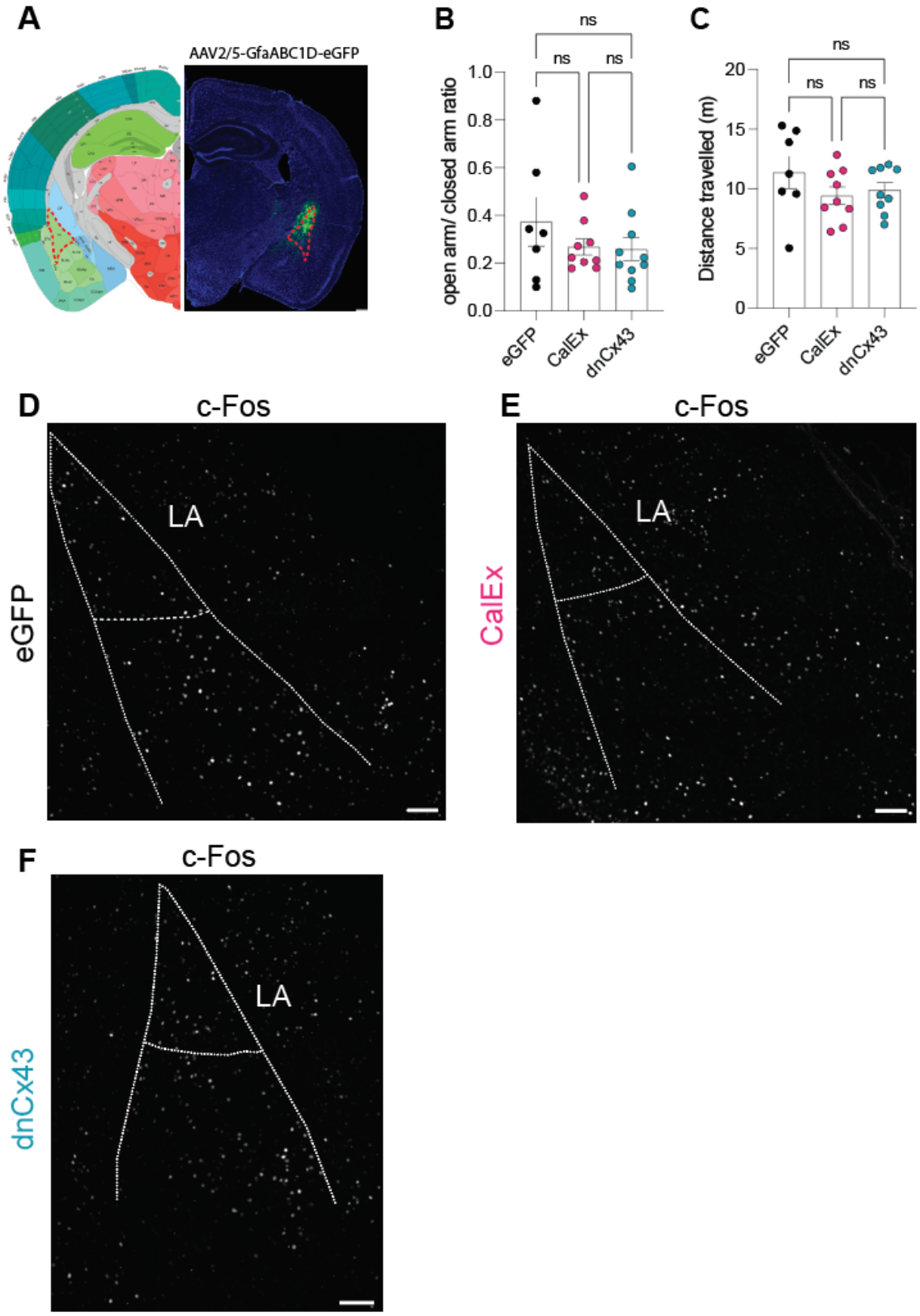

(A) Representative image of fluorescent reporter expression in lateral amygdala following AAV
730 injection. **(B)** No effect of astrocyte manipulation on open arm/closed arm duration in EPM. eGFP N=7, CalEx N=9, dnCx43 N=9 mice. **(C)** No effect of astrocyte manipulation on distance travelled in EPM. eGFP N=7, CalEx N=9, dnCx43 N=9 mice. **(D)** Representative Z-stack projection of c-FOs staining in entire LA and BLA in eGFP injected mouse 90minutes after conditioning. **(E)** Representative Z-stack projection of c-FOs staining in entire LA and BLA in CalEx injected mouse 90minutes after conditioning.
735 **(F)** Representative Z-stack projection of c-FOs staining in entire LA and BLA in dnCx43 injected mouse 90minutes after conditioning. Scale bars = 100μm

740 **Supplementary Table 1**

Figure 1	
1B	**CORT at P45** P=0.01; Naïve=50.1±6.9 ng/ml, N=9; ELS=106.1±17.2 ng/ml, N=11; mean±s.e.m
1D	**Centre/periphery ratio Naîve vs ELS** unpaired t-test, P=0.3916; Naïve=0.2585±0.05273 a.u, N=9; ELS=0.3414±0.06774 a.u, N=14; mean±s.e.m
1E	**Total distance travelled Naîve vs ELS** unpaired t-test, P=0.0454; Naïve= 17.04± 2.300 m, N=9; ELS= 22.82± 1.602 m, N=14; mean±s.e.m
1G	**Open arm/closed arm ratio Naîve vs ELS** unpaired t-test, P=0.0224; Naïve= 0.5721± 0.07017 a.u, N=18 ELS= 0.3237± 0.06254 a.u, N=11; mean±s.e.m
1H	**Total distance travelled** unpaired t-test, P=0.0224; Naïve= 8.167± 0.6223 m, N=9; ELS= 11.03± 1.079 m, N=11; mean±s.e.m
Figure 2	
2B	**Fear conditioning CS- CS+ Naîve vs ELS** Two-way ANOVA; effect of group: F (3, 393) = 64.85, P<0.0001; Tukey's multiple comparison test, Naïve CS- vs ELS CS-: P=0.3602, Naïve CS+ vs ELS CS+: P=0.5618, Naïve CS- vs Naîve CS+: P<0.0001, ELS CS- vs ELS CS+: P<0.0001, Naïve CS-=17.92±3.734 % Freezing, N=20 mice Naïve CS+=38.55±8.204 % Freezing, N=20 mice ELS CS-=13.55±3.491 % Freezing, N=17 mice ELS CS+=41.67±6.869 %Freezing, N=17 mice Mean ± s.e.m
2C	**Discrimination test Naîve vs ELS** Two-way ANOVA; effect of group: F (3, 435) = 32.36, P<0.0001; Tukey's multiple comparison test, Naïve CS- vs ELS CS-: P=0.0002, Naïve CS+ vs ELS CS+: P=0.9991, Naïve CS-=32.9±1.4 % Freezing., N=20 mice

	ELS CS-=46.03±2.9 % Freezing., N=17 mice Naïve CS+=58.77±3.2 % Freezing., N=20 mice ELS CS+=58.34±2.2 % Freezing., N=17 mice Mean±s.e.m
2D	**Discrimination index Naîve vs ELS** Two-way ANOVA; effect of group: F (1, 35) = 9.457, P=0.0041; Naïve=0.3384± 0.05986; N=20 mice ELS=0.1275± 0.03533, N=17 mice mean±s.e.m
2G	**LTP Naîve vs ELS** Unpaired t-test, P=0.0028; Naïve=142.1±8.720%, N=15; ELS=106.0±6.058, N=13; mean±s.e.m
2K	**c-Fos density Naîve vs ELS** Mann-Withney test, P<0.0001, U= 228, Naïve=17.42±0.9427 c-Fos density/$10^{-3}mm^3$, n=39 slices from N=10 mice; ELS=25.45±1.044 c-Fos density/$10^{-3}mm^3$, n=37 slices from N=10 mice; mean±s.e.m.
Figure 3	
3B	**Nuclear:cytosolic GR ratio Naîve vs ELS** P=0.026; Naïve=0.23±0.06 a.u., N=8; ELS=0.48±0.08 a.u., N=8; mean±s.e.m.
3E	**GFAP** P=0.02, unpaired t-test; Naïve=1±0.17 a.u., N=11; ELS=0.5±0.1 a.u, N=12; mean±s.e.m.
3F	**Cx43** P=0.008, unpaired t-test; Naïve=1±0.15 a.u., N=11; ELS=0.45±0.12 a.u., N=14; mean±s.e.m.
3G	**GLT-1** P=0.8, unpaired t-test; naïve=1±0.29 a.u., N=6; ELS=0.9±0.21 a.u., N=16; mean±s.e.m
Figure 4	
4C	**Fear conditioning CS- CS+ eGFP vs CalEx vs dnCx43** Two-way ANOVA; effect of group: F (5, 463) = 78.39, P<0.0001; Tukey's multiple comparison test, eGFP CS- vs dnCx43 CS-: P=0.1940, eGFP CS- vs CalEx CS-: P=0.9758, dnCx43 CS- vs CalEx CS-: P=0.7027, eGFP CS+ vs dnCx43 CS+: P=0.9536, eGFP CS+ vs CalEx CS+: P=0.6680,

	dnCx43 CS+ vs CalEx CS+: P=0.9761, eGFP CS-=11.24±1.875 % Freezing., N=12 mice CalEx CS-=9.182±2.247 % Freezing., N=11 mice dnCx43 CS-=5.515±1.936 % Freezing., N=17 mice eGFP CS+= 39.33±6.443 % Freezing., N=12 mice CalEx CS+=35.22±7.464 % Freezing., N=11 mice dnCx43 CS+=37.14±6.923 % Freezing., N=17 mice mean± s.e.m
4D	**Discrimination test eGFP vs CalEx vs dnCx43 freezing responses** Two-way ANOVA; effect of group:F (5, 457) = 25.29, P<0.0001; Tukey's multiple comparison test, eGFP CS- vs dnCx43 CS-: P=0.0293, eGFP CS- vs CalEx CS-: P<0.0001, dnCx43 vs CalEx: P=0.0005, eGFP CS+ vs dnCx43 CS+: P>0.9999, eGFP CS+ vs CalEx CS+: P>0.9999, dnCx43 CS+ vs CalEx CS+: P>0.9999 eGFP CS-= 28.73±2.342 % Freezing., N=12 mice CalEx CS-= 53.00±1.203 % freezing., N=11 mice dnCx43 CS-= 38.81±1.957 % Freezing., N=17 mice eGFP CS+= 57.79±3.314 % Freezing., N=12 mice CalEx CS+= 57.02±4.219 % Freezing., N=11 mice dnCx43 CS+= 57.32±4.344 % Freezing., N=17 mice mean± s.e.m.
4F	**LTP eGFP vs CalEx vs dnCx43** Ordinary one-way ANOVA, group effect: F (2, 31) = 4.221, P=0.0239; Uncorrected Fisher's LSD, eGFP vs CalEx: P=0.0408, eGFP vs dnCx43: P=0.0207, CalEx vs dnCx43: P=0.8848, eGFP=139.0±17.70 % baseline., N=5; CalEx=100.3±7.485 % baseline., N=9; dnCx43=98.31±8.635 % baseline., N=16; mean± s.e.m
4H	**c-Fos density eGFP vs CalEx vs dnCx43** Ordinary one-way ANOVA, group effect: F (2, 43) = 14.91, P<0.0001; Tukey's multiple comparison test, eGFP vs CalEx: P<0.0001, eGFP vs dnCx43: P=0.0005, CalEx vs dnCx43: P=0.8807

	eGFP=17.97±0.8195 c-Fos density/$10^{-3}mm^{3.}$, n=17 slices from N=5 mice; CalEx=27.66±1.398 c-Fos density/$10^{-3}mm^{3.}$, n=17 from N=5 mice; dnCx43=26.65±2.173 c-Fos density/$10^{-3}mm^{3.}$, n=12 slices from N=5 mice; mean±s.e.m
Supplementary figures	
S1A	**Fear conditioning CS- CS+ Females vs Males** Two-way ANOVA; effect of group: F (3, 99) = 15.54, P<0.000; Tukey's multiple comparison test, Female CS- vs Male CS-: P=0.2521, Female CS+ vs Male CS+: P=0.8432, Female CS- vs Female CS+: P=0.0017, Male CS- vs Male CS+: P<0.0001, Female CS-=23.90±5.126 % Freezing., N=7 mice Male CS-=16.31±3.339 % Freezing., N=8 mice, Female CS+=39.49±8.089 % Freezing., N=7 mice, Male CS+=36.1±8.544 % Freezing., N=8 mice, Mean±s.e.m.
S1B	**Discrimination test Females vs Males** Two-way ANOVA; effect of group: F (3, 156) = 13.92, P<0.0001; Tukey's multiple comparison test, Female CS- vs Male CS-: P=0.3956, Female CS+ vs Male CS+: P=0.8851, Female CS- vs Female CS+: P=0.0011, Male CS- vs Male CS+: P<0.0001, Female CS-=36.79±1.241 % Freezing., N=7 mice, Male CS-=27.97±2.183 % Freezing., N=8 mice, Female CS+=58.83±4.849 % Freezing., N=7 mice, Male CS+=54.75±2.580 % Freezing., N=8 mice, Mean±s.e.m.
S1C	**Discrimination index Females vs Males** Two-way ANOVA; effect of group: F (1, 13) = 0.03698, P=0.8505; Female DI=0.3320±0.06280 a.u., N=7 mice, Male DI=0.3627±0.06860 a.u., N=8 mice, Mean±s.e.m.
S2B	**Open arm/Closed arm ratio eGFP vs CalEx vs dnCx43** Two-way ANOVA; effect of group: F (2, 23) = 0.9903, P=0.3867; Tukey's multiple comparison test, eGFP vs CalEx: P=0.4961, eGFP vs dnCx43: P=0.3919, CalEx vs dnCx43: P=0.9783,

	eGFP=0.3739±0.1036 a.u., N=7 mice, CalEx=0.2679±0.03393 a.u., N=9 mice, dnCx43=0.2576±0.05335a.u., N=9 mice, Mean±s.e.m.
S2C	**Distance traveled eGFP vs CalEx vs dnCx43** Ordinary one-way ANOVA; effect of group: F (2, 24) = 1.304, P=0.2901; Tukey's multiple comparison test, eGFP vs CalEx: P=0.2722, eGFP vs dnCx43: P=0.4726, CalEx vs dnCx43: P=0.9265, eGFP=11.38±1.379 m., N=7 mice, CalEx=9.482±0.5968 m., N=9 mice, dnCx43=9.898±0.6352 m., N=9 mice, Mean±s.e.m.